CR 151221

FINAL REPORT

SPACE SHUTTLE CAVITY ASSESSMENT TEST PROGRAM

Report No. T169- 66

Dec. 31, 1976

Prepared Under Contract NAS 9-10534

for

NASA JOHNSON SPACE CENTER

CREW SYSTEMS DIVISION

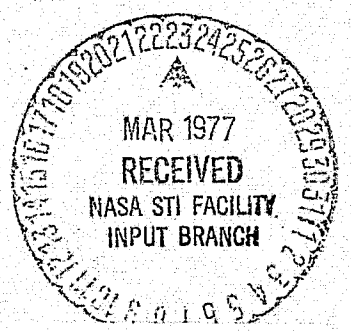

(NASA-CR-151221) SPACE SHUTTLE CAVITY ASSESSMENT TEST PROGRAM Final Report (Vought Corp., Dallas, Tex.) 96 p HC A05/MF A01 CSCL 22B

N77-19148

Unclas
G3/16 20502

VOUGHT CORPORATION

an LTV Company

FINAL REPORT

SPACE SHUTTLE CAVITY ASSESSMENT TEST PROGRAM

Report No. T169- 66

Dec. 31, 1976

Prepared Under Contract NAS 9-10534

for

NASA JOHNSON SPACE CENTER

CREW SYSTEMS DIVISION

PREPARED BY:

P. B. Scheps
Principal Investigator

REVIEWED BY:

J. A. Oren
Environmental Systems

J. Utterback, Supervisor
Thermal & Environmental Systems

APPROVED BY:

R. L. Cox
Thermal R&D

CONTENTS

List of Figures

1.0 INTRODUCTION

Shuttle Orbiter Heat Rejection System (OHRS) development testing was accomplished at Johnson Space Center (JSC) during 1975 and 1976. This series of tests provided data essential in establishing final design of the OHRS radiator hardware and associated control techniques.

The test program was conducted jointly by NASA; Rockwell International, the Shuttle prime contractor; and the Vought Corporation, the radiator subcontractor. Vought, under contract NAS 9-10534, provided the radiator test articles and planning and analysis support. Basic requirements for these tests were documented in "Orbiter Heat Rejection System Test Requirements Document,"Johnson Space Center Report No. CSD-SH-51,3/75.

The purpose of this report is to document the first three tests in the series. These three tests, which took place between March 3 and June 20, 1975, were distinct from subsequent testing in that the test article was a non-flowing radiator configuration simulator known as the Cavity Assessment Test Article (CATA).

1.1 CAVITY ASSESSMENT TEST SUMMARY

In order to obtain basic radiation properties of the radiator/payload bay door cavity, three tests were conducted on a full-size structural simulator of the cavity. The testing was done in three phases, as follows:

a. March 3-28, 1975, (four weeks); Chamber B; CATA used for determination of exchange factors, absorbed solar flux, and door covering influences.

b. April 22-May 1, 1975, (two weeks); Chamber A; quartz lamp array calibrated to provide IR flux distribution on CATA.

c. June 16-20, 1975, (one week); Chamber B; retest with radiometer array for background flux measurement.

1.2 TEST OBJECTIVES

The overall objective of the test series was to provide experimental values of exchange factors and absorbed solar and IR flux which could be used in subsequent testing of a full scale flowing radiator panel and/or system. Thus, in a sense, the entire cavity assessment test program was a calibration phase for the overall radiator test program. Figure 1-1 illustrates this rationale.

More specifically, the objectives of the test program were to:

a. Measure exchange factors from the radiator and door to space.

b. Measure exchange factors between the radiator and door.

c. Observe total absorbed heat as a function of incident solar impingement angle.

d. Measure the effects of a wider cavity angle on (a), (b), (c) above.

e. Evaluate silver/Teflon coating and adhesive under realistic environments (to be documented separately).

f. Gather data suitable for thermal model correlation in preparation for flowing panel testing.

g. Evaluate effect of alternative door coating materials.

FIGURE 1-1

CAVITY ASSESSMENT TEST

SEQUENCE

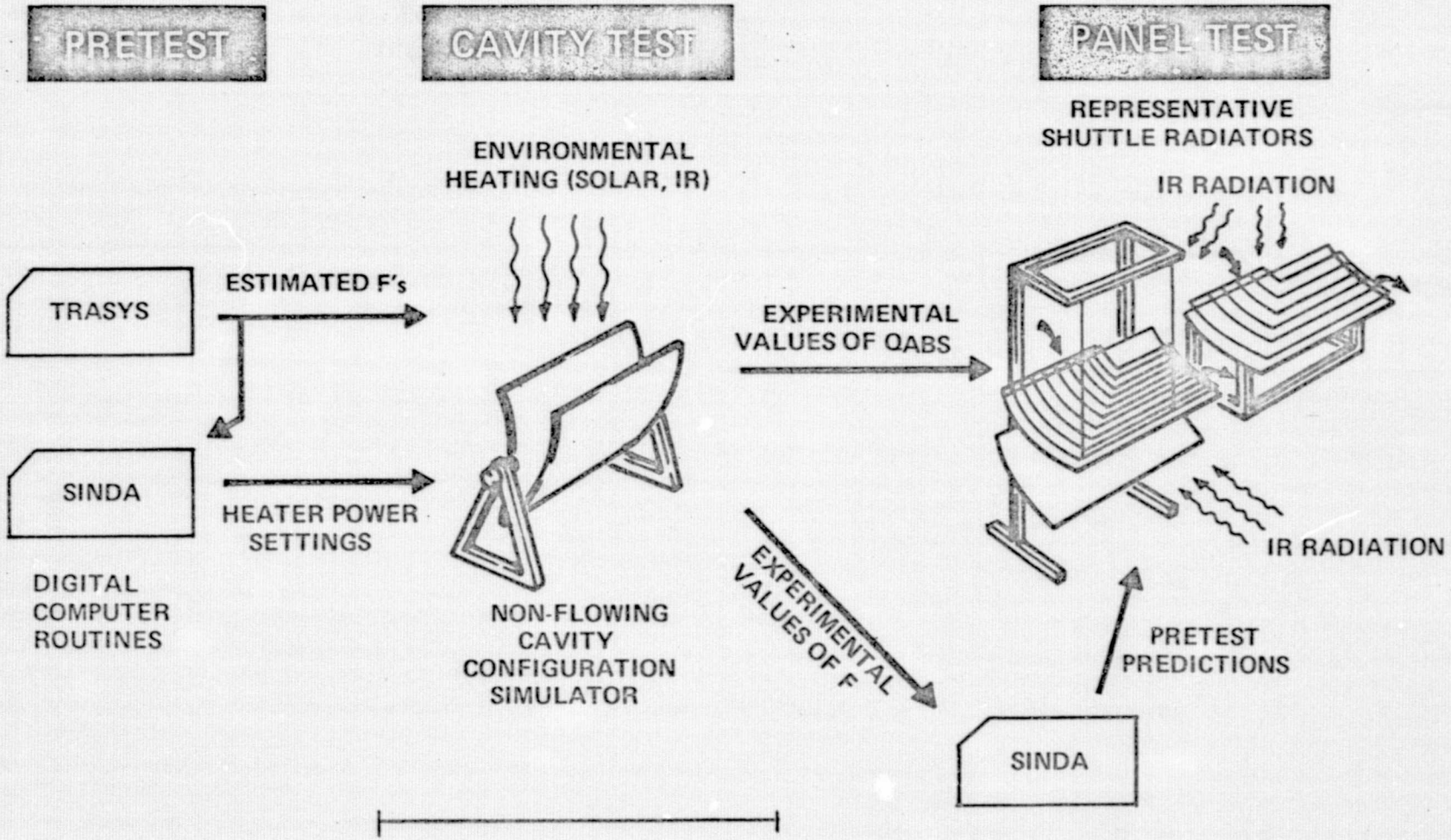

2.0 BACKGROUND

This section describes the Orbiter Heat Rejection System(OHRS) and provides background information on the rationale for the test series. In addition, the unique properties of the radiator-to-payload bay door cavity are discussed, and data on the silver/Teflon coating material is presented.

2.1 ORBITER HEAT REJECTION SYSTEM DESIGN

The operational OHRS will consist of three devices to reject the heat loads both internally generated and absorbed from the environment; namely, space radiators, flash evaporator system(FES),and ammonia boiler. Supplemental heat rejection capacity will be provided on the ground by a Ground Support Equipment (GSE) heat exchanger.

During on-orbit operation, heat rejection will be accomplished primarily by the space radiators, supplemented by water evaporation through the FES (Figure 2-1). The orbiter radiator configuration consists of 6 or 8 panels to be mounted to the payload bay doors as shown in Figure 2-2. The two forward panels on each side are to be deployed away from the doors to increase the heat rejection capacity. Freon flow to the panels will be regulated by two downstream temperature control valves. The valves will bypass a portion of the flow to regulate the radiator outlet temperature to either of two temperature set points (38 F and 58 $^{\circ}$F). The set point temperature will depend upon the quantity of water in the fuel cell water storage system. As excessive water accumulates in the holding tank the set point will be increased to 58 $^{\circ}$F, thereby reducing the amount of heat rejection from the radiators. Water evaporated in the flash evaporator top-off

FIGURE 2-1

SIMPLIFIED SCHEMATIC OF ORBITER HEAT REJECTION SYSTEM

(ONE OF TWO REDUNDANT LOOPS SHOWN)

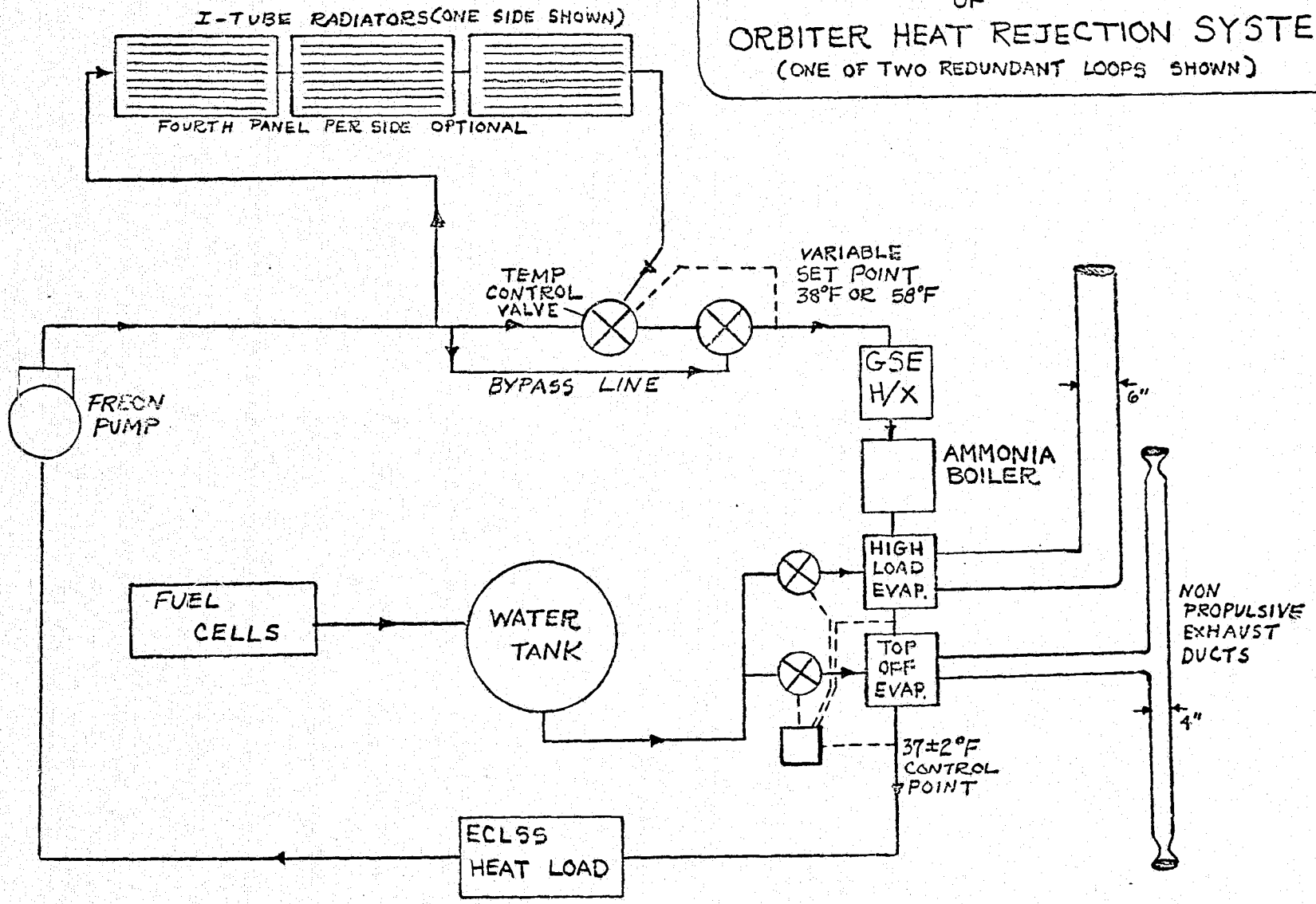

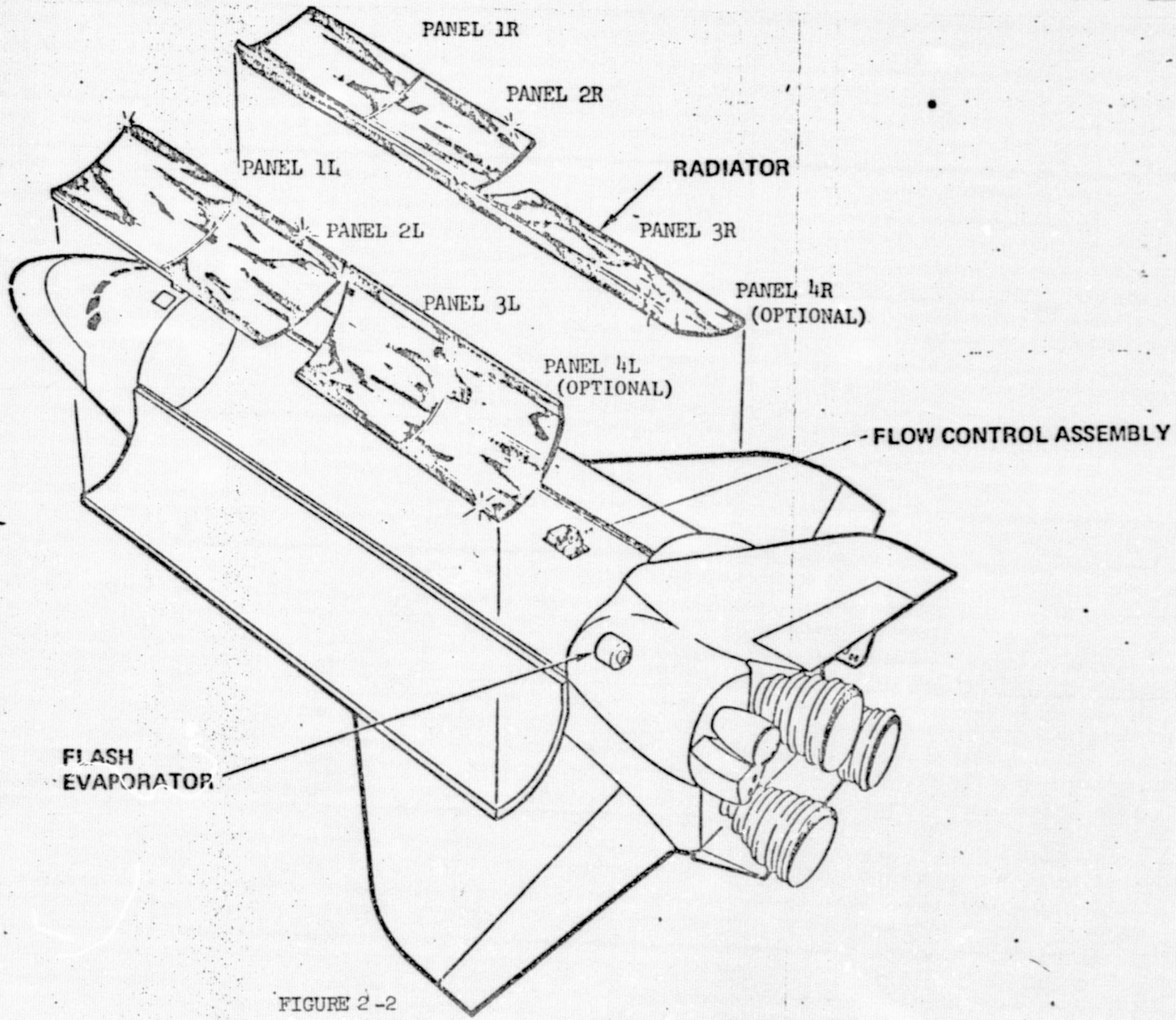

I TUBE PANEL

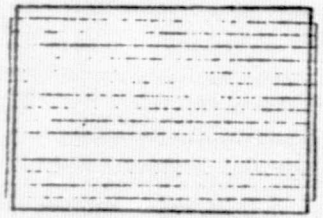

FIGURE 2-2

SPACE SHUTTLE ORBITER RADIATOR CONFIGURATION

section will lower the freon temperature to 37±2°F until the holding tank level decreases, at which time the control valve will be reset to 38°F. Should on-orbit heat loads increase such that the radiator outlet temperature cannot be maintained at 38±2° with full flow through the radiators, the flash evaporator will activate as necessary to control the temperature of the freon supplied to the vehicle at 37°F. The water is rejected from the flash evaporator through a set of non-propulsive sonic nozzles to minimize the particle and gas contamination of the space environment surrounding the orbiter.

In addition to providing supplemental heat rejection capacity during on-orbit operation, the FES will provide the sole means of heat rejection for the orbiter above an altitude of 140,000 feet during ascent and above 100,000 feet during reentry. Below 100,000 feet the ammonia boiler is activated to provide cooling during reentry and through the post landing phase.

2.2 CAVITY DESIGN

The orbiter radiators are stored in the payload bay for protection during launch and re-entry, and are deployed on-orbit. Deployment is accomplished by opening the payload bay doors, and rotating the four forward panels away from the doors along the hinge line to form the operating configuration shown in Fig. 2-2. Since payload volume is at a premium, the radiators must conform to the shape of the doors and very little panel/door configuration design flexibility is available. The resulting forward panel/door cross-section (Figure 2-3) presents several challenging thermal design and analysis problems. Solutions to these problems were the subject of a test program, conducted by NASA-Johnson Space Center, which is described in this report.

FIGURE 2-3

CROSS-SECTIONAL VIEW OF CAVITY

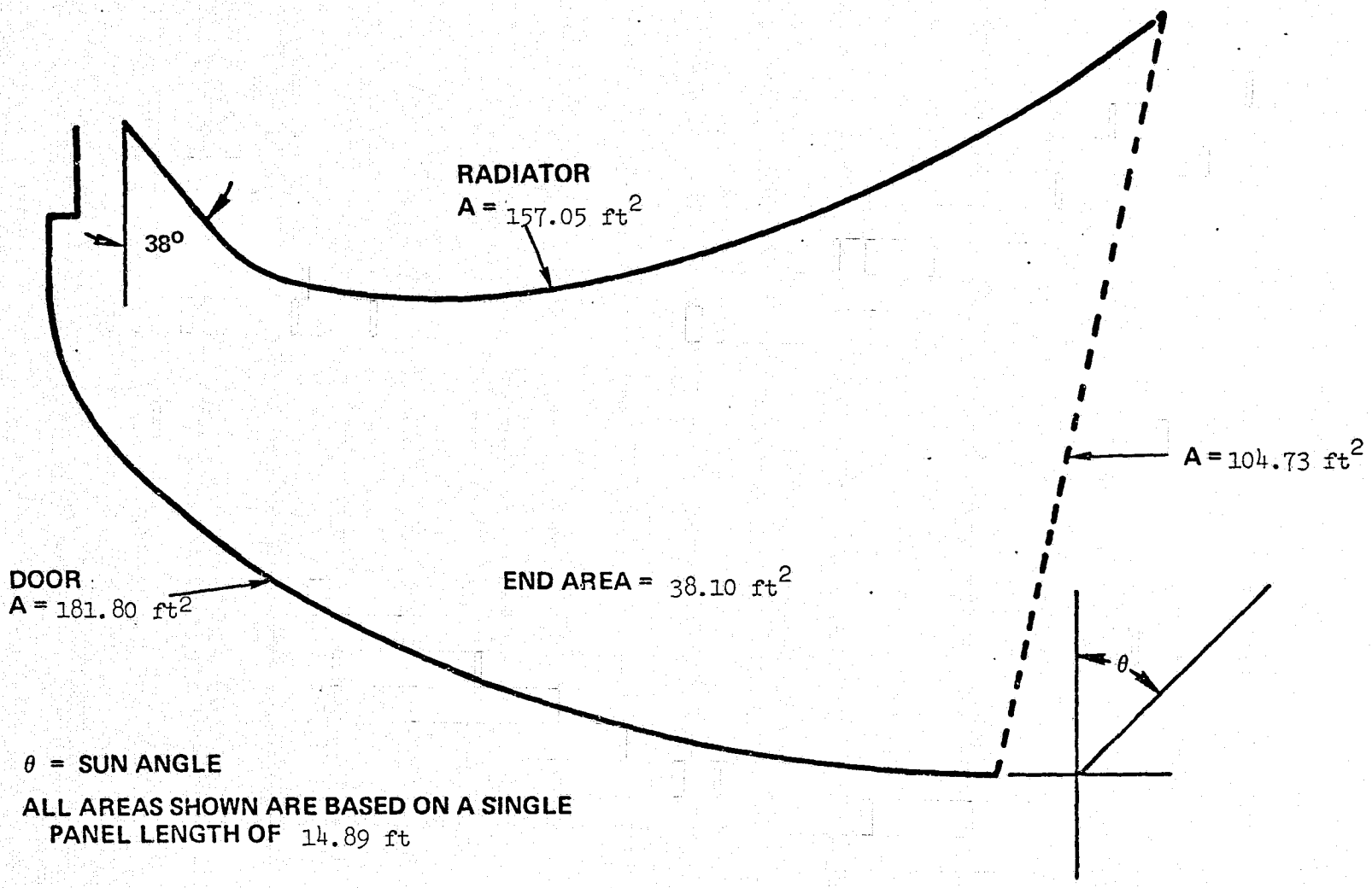

The orbiter radiator performance depends on the radiant interchange between the panel and door, the net energy leaving the panel/door "cavity", and the absorption of energy entering the cavity. The thermal control coating used on the radiator panels and forward door segments is silver/Teflon (Figure 2-4) which provides a low solar absorptivity and high emissivity. This coating exhibits highly specular reflections in both the solar and infrared wave lengths. Although little data are available on directional emittance, a hemispherical/normal emittance ratio of 0.945 has been obtained from electromagnetic theory for an opaque dielectric, indicating that the material is a diffuse emitter.

Solutions are available in the literature for cavities with specular flat surfaces and for specialized enclosures with specular curved surfaces e.g., cylinders and cones. None of these solutions adequately represent the radiator/door cavity which is formed by two curved surfaces only one of which is heated. General radiation heat transfer computer routines are available in the industry for diffuse surfaces. The only known general routine for specular surfaces available at the time of this study is that developed by the Martin Marietta Company which considers only one reflection. The Boeing Company apparently has a proprietary general routine for specular enclosures.

FIGURE 2 -4

SILVER/TEFLON DETAIL

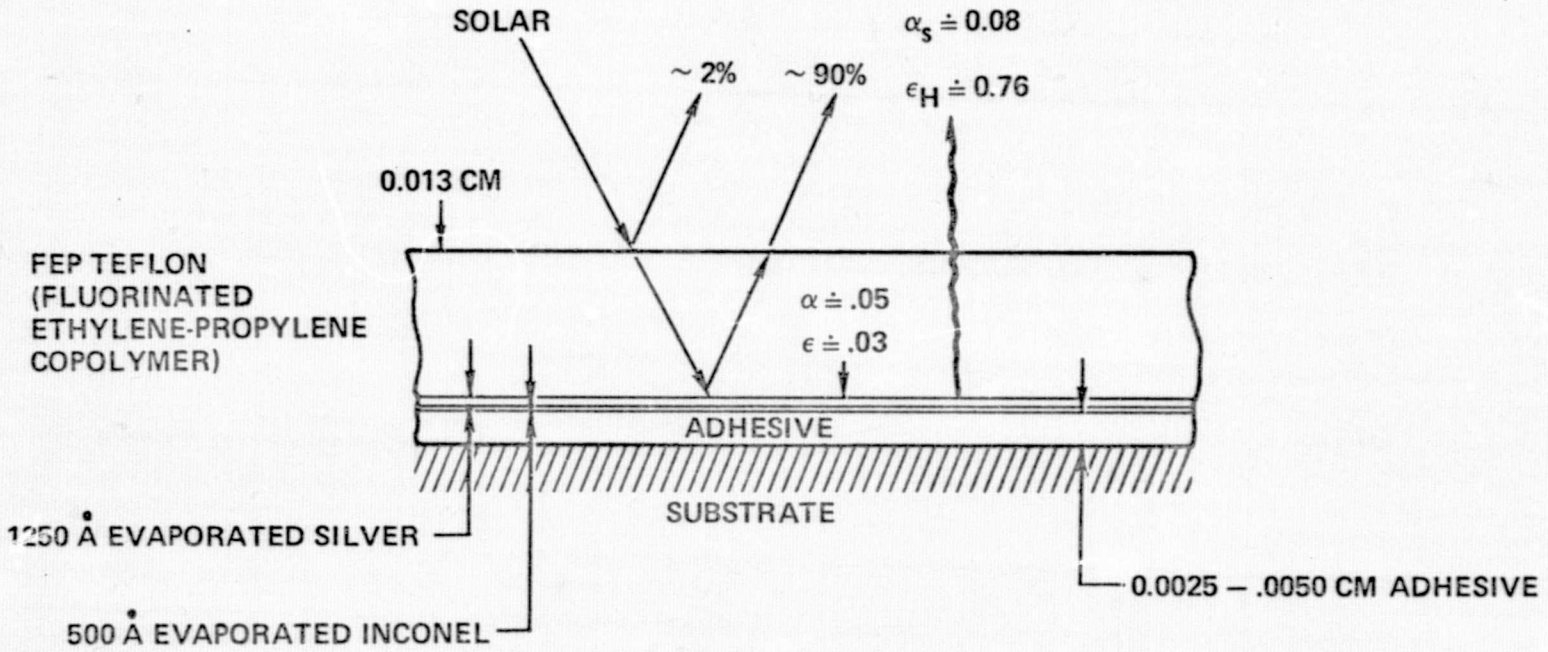

OPERATING PRINCIPLE

- SUNLIGHT IS LARGELY TRANSMITTED BY TEFLON AND REFLECTED AT SILVER INTERFACE. ABSORPTION IN TEFLON IS MINOR, BUT INCREASES WITH EXPOSURE TO DAMAGING SPACE RADIATION.
- INFRARED EMISSION ORIGINATES THROUGHOUT TEFLON VOLUME AND IS A STRONG FUNCTION OF TEFLON THICKNESS. A 0.013 CM THICKNESS HAS ABOUT 94% THE EMITTANCE OF AN INFINITE BODY.
- INCONEL SERVES AS A CONTAMINATION BARRIER FOR THE SILVER AND ADDS OPACITY TO THE SILVER FILM.

3.0 TEST ARTICLE DESCRIPTION

3.1 CAVITY SIMULATOR

The test article for this series of tests was a full-scale representation of a deployed radiator panel and a 15 ft. section of the payload bay door (Figure 3-1). The angle between the panel simulator and door (the deployment angle) was fixed during each phase of the test, but could be modified with the test chamber at atmospheric pressure by changing the length of the struts (Figure 3-2) joining the outboard corners of the panel and door. For the majority of the testing reported herein, the deployment angle was 38[1] degrees. Additional test points investigated a wider cavity opening as a means of increasing total heat rejection.

The entire test fixture was automatically rotatable from outside the chamber, to allow for simulation of solar inpingement at different angles. A TELSYN servomechanism and digital readout gave continuous readings on test article angular position.

Figures 3-3 and 3-4 are photographs of the chain drive arrangement which provided the rotational capability for the test article. The angular markings on the sprocket pictured in Figure 3-3 were visible from the manlock viewing port and could also be used to align the test article.

The door, like the panel simulator, was coated with silver/Teflon material, and included nine ring-frames, (Figure 3-5) or T-shaped beams, reaching from hinge line to outboard edge. The tops of these beams were also

---

[1] Subsequent to this testing, the baseline deployment angle was redefined to 35.5°

FIGURE 3-1

CAVITY ASSESSMENT TEST ARTICLE

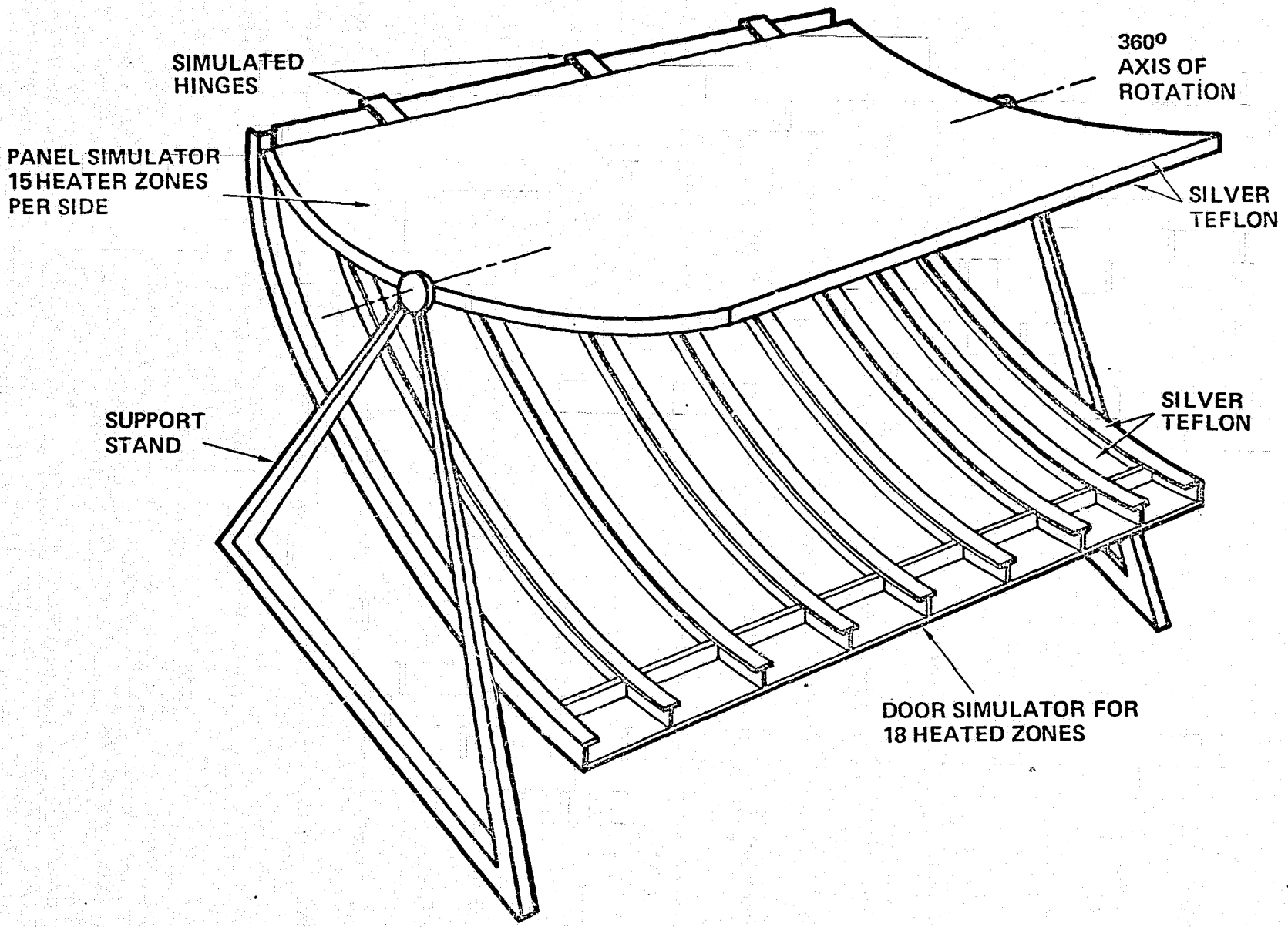

FIGURE 3-2

PHOTOGRAPH OF TEST ARTICLE

FIGURE 3-3

CLOSE-UP OF SPROCKET ON TEST ARTICLE

FIGURE 3-4

TEST ARTICLE DRIVE MOTOR AND LINKAGE

FIGURE 3-5
VIEW OF CAVITY WITH BEAMS IN PLACE

coated with silver/Teflon. The entire set of beams was easily removable, and a portion of the testing was dedicated to evaluating the differences in radiation properties which would result from neglecting the presence of the beams.

During a portion of the test, a white blanket was secured over the door to evaluate the effect of a diffuse surface coating on the net radiation trapping in the cavity. The blanket was constructed of beta cloth bonded to a thin aluminum sheet, which was then rigidly attached to the door. Figure 3-6 is a photograph of the white blanket during installation. Results will be discussed in section 6.5

The actual construction of the panel and door simulator is shown in Figure 3-7. For this test series, the panel simulator was a geometrically-representative structure whose surface was electrically heated in discrete zones. There were 15 of these zones on each side of the radiator simulator (numbered 1 through 30). The door was also designed to be independently heated through 18 zones (numbered 31 through 48). The portion of each beam that was over a door zone was also individually temperature-controlled.

Each zone consisted of a Cox 128 heater bonded to one side of a 0.16 CM aluminum sheet, and mounted on a structure which conformed to the Shuttle contour. The side of the aluminum sheet that faced "outward," or into the cavity, was covered with silver/Teflon. Three thermocouples per zone were also attached to the aluminum during construction. Each zone was

FIGURE 3-6

BETA CLOTH BLANKET ON PAYLOAD BAY DOOR

FIGURE 3-7

TEST ARTICLE CONSTRUCTION DETAIL

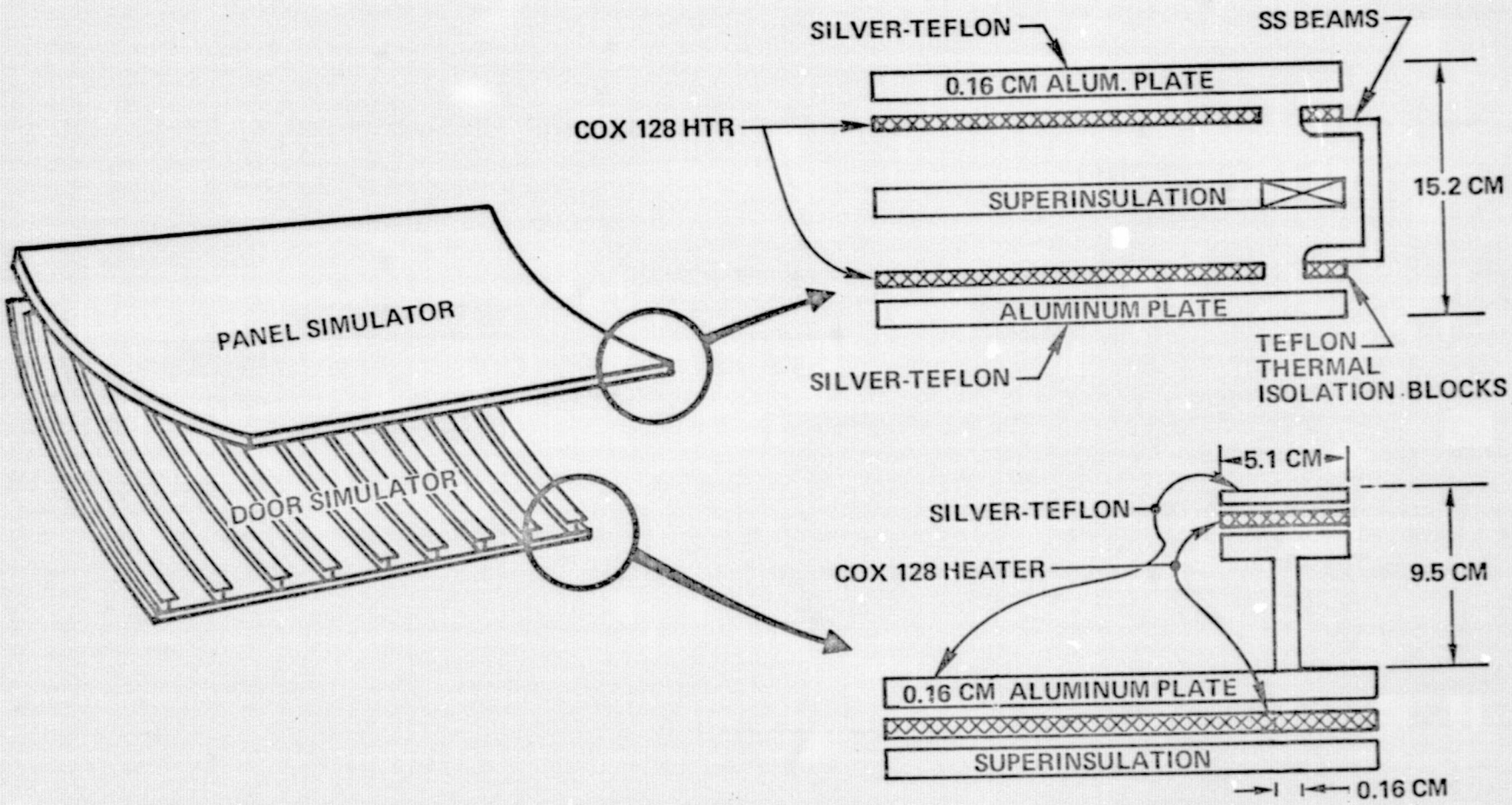

mounted on thermal isolation blocks and thermally insulated against heat leak with 10-20 layers of aluminized mylar superinsulation.

Zone temperatures were controlled either manually or by a power supply whose output was automatically made proportional to the difference between the average temperature of the zone and the desired temperature. It had been speculated that the smaller, inboard zones, with strong radiation "views" of each other, could not be stably controlled with such an automatic system. However, the system instability did not occur, and the temperature-seeking logic provided rapid approach to steady-state conditions.

3.2 ENVIRONMENT SIMULATION/MEASUREMENT

3.2.1 Chamber B

Solar simulation was accomplished by an array of Xenon lamps mounted in the top of the chamber. These lamps produced a solar beam of sufficient width and breadth (approximately 9 x 15 ft) to completely illuminate the cavity opening for all rotation angles. Scanning radiometers were mounted such that they could measure the entire solar beam and provide a 2 in. x 2 in. matrix of flux data to insure representative uniformity and intensity of the solar simulation.

During the cavity background test, 10 radiometers were mounted on a frame that was attached to the test article and rotated with it. Figure 3-8 shows the location and numbering of these radiometers. Figure 3-9 is a

FIGURE 3-8

LOCATION OF RADIOMETERS

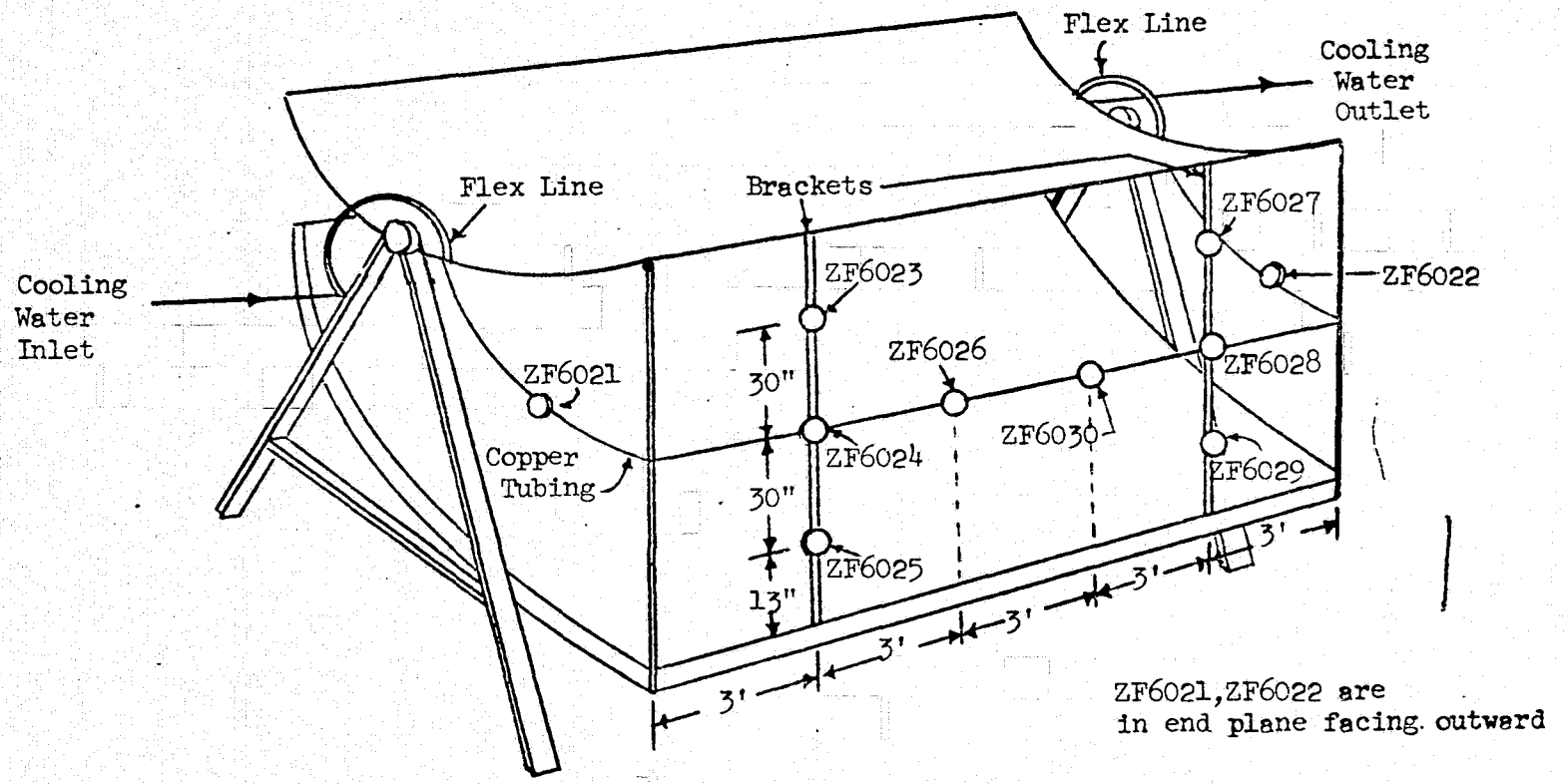

photograph of the radiometers in place prior to the test. The support frame was actually copper tubing through which water was continually pumped to maintain the radiometers at a constant temperature.

The radiometers were utilized to measure the chamber background flux, due to emission from the chamber walls and solar mirrors, and due to reflections. The test article, with radiometers attached, was scanned through the appropriate range of angles, and the radiometer response noted for each angle.

3.2.2 Chamber A

Environment for the Chamber A testing was provided by a 9-lamp quartz lamp array (QLA) mounted above the test article. In addition, the cavity opening was covered by a variable-temperature IR panel. Figure 3-10 is a schematic diagram of this arrangement. Each quartz lamp was individually-powered to accomplish a large range of environmental simulation.

Each quartz lamp was 18 feet long and thus overlapped to test article by 1.5 feet on each end. The same QLA was used to provide environment for subsequent tests using flowing radiators. A second QLA of similar design was also constructed and was present in the chamber mounted over a radiometer array. Data from this test article was used to adjust fluxes to the cavity simulator, but final flux values were calculated using an energy balance discussed in later sections.

FIGURE 3-9

RADIOMETER ARRAY ATTACHED TO TEST ARTICLE

FIGURE 3-10

TEST ARTICLE CONFIGURATION FOR CHAMBER

A IR TEST PHASE

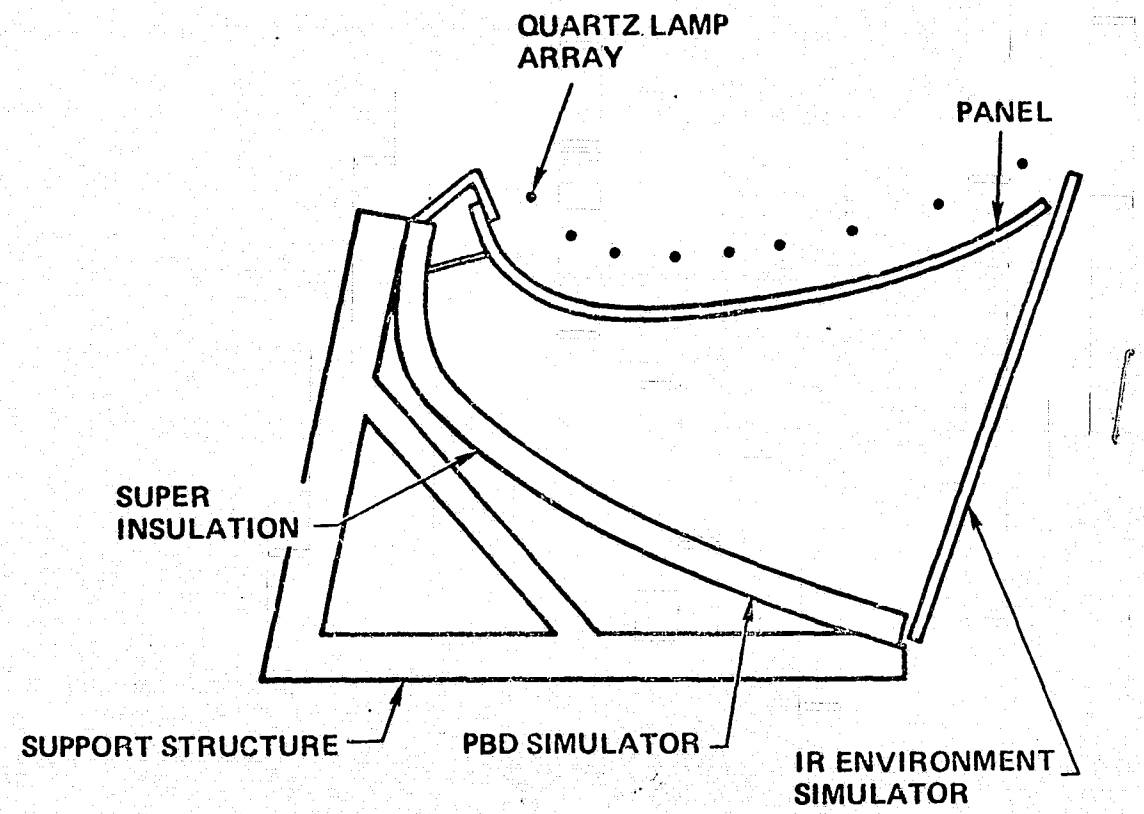

37

3.3 INSTRUMENTATION

The basic test article instrumentation consisted of thermocouples bonded to the back side of each zone. There were three thermocouples per zone, mounted on the longitudinal centerline and equally spaced. Figures 3-11, 3-12, and 3-13 give the thermocouple locations, numbers, and heater instrumentation numbers for the top side of the radiator simulator, the bottom side of the radiator simulator, and the door,.respectively.

The current to each heater was measured and converted to total power dissipation by the relationship $P=I^2R$ where R is heater resistance. The values of R, including their dependence on temperature, were measured pre-test and available automatically through the on-line computing facilities at SESL. Table 3-1 lists the value of each heater resistance.

Zone temperature control was accomplished manually during the early phases of the testing, and a computer-control system added midway through the series. With manual control, the facility engineer adjusted current until stable temperatures were reached. A waiting period was required to ensure steady-state.

With the automatic system, the current was continually adjusted to hold a particular desired temperature distribution. The current (and power) were variable under this method as the computer continually adjusted in response to an error signal proportional to the difference between actual and desired temperature. To obtain total power dissipation, logic was added to the program to time-average the current before converting it to power dissipation.

FIGURE 3-11

RADIOMETER LOCATIONS-TOP OF PANEL

UPPER SURFACE RADIATOR

ZN 1 HTR # CF 3401 CA1001 CA1002 CA1003	ZN 6 HTR # CF 3406 PG 7 LN 9 MOD 45 CA1016 PG 1 LN 9 CA1017 PG 1 LN 10 CA1018 PG 1 LN 11	ZN11 HTR # CF 3411 PG 7 LN 6 MOD 46 CA1031 PG 1 LN 15 CA1032 PG 1 LN 16 CA1033 PG 1 LN 17
ZN 2 HTR # CF 3402 CA1004 CA1005 CA1006	ZN 7 HTR # CF 3407 PG 7 LN 10 MOD 48 CA1019 PG 1 LN 15 CA1020 PG 1 LN 16 CA1021 PG 1 LN 17	ZN12 HTR # CF 3412 PG 7 LN 7 MOD 49 CA1034 PG 1 LN 21 CA1035 PG 1 LN 22 CA1036 PG 1 LN 23
ZN 3 HTR # CF 3403 CA1007 CA1008 CA1009	ZN 8 HTR # CF 3408 PG 7 LN 8 MOD 51 CA1022 PG 1 LN 21 CA1023 PG 1 LN 22 CA1024 PG 1 LN 23	ZN13 HTR # CF 3413 PG 7 LN 8 MOD 52 CA1037 PG 1 LN 3 CA1038 PG 1 LN 4 CA1039 PG 1 LN 5
ZN 4 HTR # CF 3404 HTR # CF 3464 CA1010 CA1011 CA1012	ZN 9 HTR # CF 3409 PG 7 LN 2 HTR # CF 3466 PG 7 LN 2 MOD 111 MOD 113 CA1025 PG 1 LN 3 CA1026 PG 1 LN 4 CA1027 PG 1 LN 5	ZN14 HTR # CF 3414 PG 7 LN 9 HTR # CF 3468 PG 7 LN 10 MOD 115 MOD 117 CA1040 PG 1 LN 9 CA1041 PG 1 LN 10 CA1042 PG 1 LN 11
ZN 5 HTR # CF 3405 HTR # CF 3465 CA1013 CA1014 CA1015	ZN10 HTR # CF 3410 PG 7 LN 4 HTR # CF 3467 PG 7 LN 5 MOD 112 MOD 114 CA1028 PG 1 LN 9 CA1029 PG 1 LN 10 CA1030 PG 1 LN 11	ZN15 HTR # CF 3415 PG 7 LN 11 HTR # CF 3469 PG 7 LN 12 MOD 116 MOD 118 CA1043 PG 1 LN 15 CA1044 PG 1 LN 16 CA1045 PG 1 LN 17

FIGURE 3-12
RADIOMETER LOCATIONS-BOTTOM OF PANEL

LOWER SURFACE RADIATOR

ZN20 HTR # CF3420 PG 7 LN 6 — MOD 88, MOD 89 CB1113 PG 2 LN 3 — CB1114 PG 2 LN 4 — CB1115 PG 2 LN 5	ZN25 HTR # CF3425 PG 7 LN 2, HTR # CF3471 PG 7 LN 3 — MOD 91, MOD 92 CB1128 PG 2 LN 9 — CB1129 PG 2 LN 10 — CB1130 PG 2 LN 11	ZN30 HTR # CF3430 PG 7 LN 8, HTR # CF3472 PG 7 LN 9 — MOD 94, MOD 95 CB1143 PG 2 LN 15 — CB1144 PG 2 LN 16 — CB1145 PG 2 LN 17
ZN19 HTR # CF3419 PG 7 LN 5 — MOD 87 CB1110 PG 2 LN 21 — CB1111 PG 2 LN 22 — CB1112 PG 2 LN 23	ZN24 HTR # CF3424 PG 7 LN 11 — MOD 90 CB1125 PG 2 LN 3 — CB1126 PG 2 LN 4 — CB1127 PG 2 LN 5	ZN29 HTR # CF3429 PG 7 LN 7 — MOD 93 CB1140 PG 2 LN 9 — CB1141 PG 2 LN 10 — CB1142 PG 2 LN 11
ZN18 HTR # CF3418 PG 7 LN 4 — MOD 37 CB1107 PG 2 LN 15 — CB1108 PG 2 LN 16 — CB1109 PG 2 LN 17	ZN23 HTR # CF3423 PG 7 LN 10 — MOD 39 CB1122 PG 2 LN 21 — CB1123 PG 2 LN 22 — CB1124 PG 2 LN 23	ZN28 HTR # CF3428 PG 7 LN 6 — MOD 41 CB1137 PG 2 LN 3 — CB1138 PG 2 LN 4 — CB1139 PG 2 LN 5
ZN17 HTR # CF3417 PG 7 LN 3 — MOD 36 CB1104 PG 2 LN 9 — CB1105 PG 2 LN 10 — CB1106 PG 2 LN 11	ZN22 HTR # CF3422 PG 7 LN 9 — MOD 38 CB1119 PG 2 LN 15 — CB1120 PG 2 LN 16 — CB1121 PG 2 LN 17	ZN27 HTR # CF3427 PG 7 LN 5 — MOD 40 CB1134 PG 2 LN 21 — CB1135 PG 2 LN 22 — CB1136 PG 2 LN 23
ZN16 HTR # CF3416 PG 7 LN 2 — MOD 33 CB1101 PG 2 LN 3 — CB1102 PG 2 LN 4 — CB1103 PG 2 LN 5	ZN21 HTR # CF3421 PG 7 LN 8 — MOD 34 CB1116 PG 2 LN 9 — CB1117 PG 2 LN 10 — CB1118 PG 2 LN 11	ZN26 HTR # CF3426 PG 7 LN 4 — MOD 35 CB1131 PG 2 LN 15 — CB1132 PG 2 LN 16 — CB1133 PG 2 LN 17

FIGURE 3-13
RADIOMETER LOCATIONS-PAYLOAD BAY DOOR

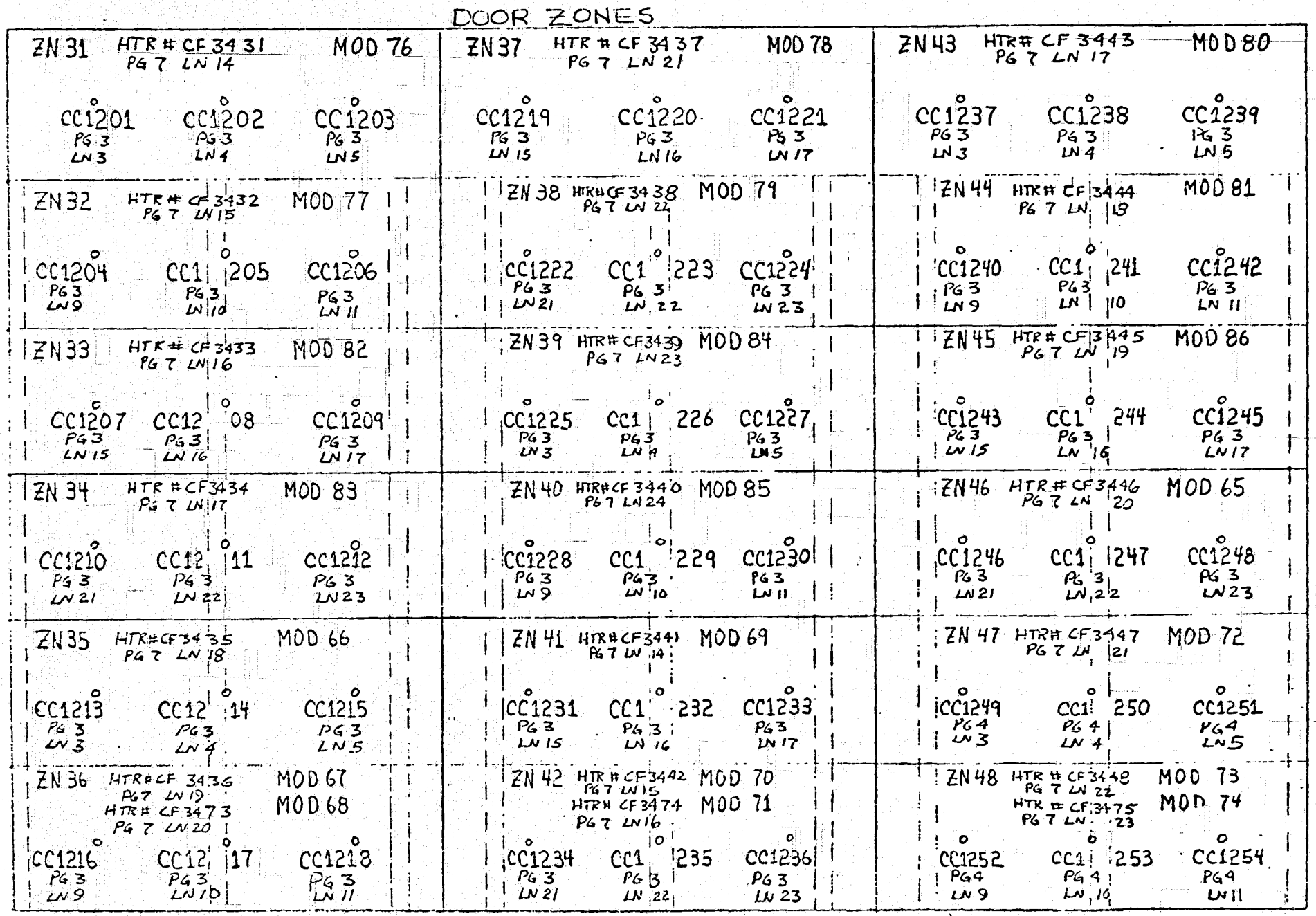

TABLE 3-1

RESISTANCE OF ZONE HEATERS

Zone	RESISTANCE OF ZONE HEATERS					
	40 deg		80 deg		120 deg	
1	17	.669	19	.119	20	.983
2	24	.155	26	.137	28	.665
3	12	.163	13	.161	14	.444
4	17	.574	18	.036	18	.616
5	12	.423	13	.442	14	.753
6	17	.699	19	.151	21	.018
7	24	.052	26	.026	28	.564
8	12	.149	13	.146	14	.428
9	17	.603	18	.056	18	.646
10	12	.453	13	.475	14	.789
11	17	.581	19	.132	20	.997
12	24	.360	26	.354	28	.929
13	12	.164	13	.162	14	.445
14	17	.519	17	.973	18	.557
15	12	.442	13	.463	14	.776
16	17	.738	19	.194	21	.065
17	24	.032	26	.004	28	.539
18	12	.167	13	.165	14	.449
19	8	.817	9	.046	9	.340
20	12	.398	13	.415	14	.723
21	17	.773	19	.231	21	.106
22	24	.054	26	.028	28	.566
23	12	.176	13	.175	14	.460
24	8	.785	9	.013	9	.306
25	12	.421	13	.446	14	.750
26	17	.753	19	.210	21	.083
27	24	.096	26	.073	28	.615
28	12	.152	13	.149	14	.431
29	8	.812	9	.041	9	.335
30	12	.384	13	.400	14	.707
31	30	.789	33	.315	36	.563
32	28	.694	31	.049	34	.076
33	17	.675	19	.125	20	.990
34	10	.508	11	.370	12	.479
35	8	.687	8	.912	9	.202
36	10	.591	11	.460	12	.577
37	30	.890	33	.425	36	.684
38	28	.612	30	.960	33	.979
39	17	.690	19	.142	21	.008
40	10	.480	11	.340	12	.446
41	8	.552	8	.774	9	.059
42	10	.586	11	.455	12	.572
43	30	.855	33	.387	36	.642
44	28	.701	31	.056	34	.084
45	17	.738	19	.193	21	.064
46	10	.480	11	.340	12	.446
47	8	.669	8	.894	9	.183
48	10	.507	11	.477	12	.596

Htr	Zone	40 deg	
64	4	17	.564
65	5	12	.426
66	9	17	.560
67	10	12	.469
68	14	17	.617
69	15	12	.379
70	20	12	.388
71	25	12	.386
72	30	12	.393
73	36	10	.582
74	42	10	.590
75	48	10	.591

Htr	Zone	80 deg	
64	4	18	.020
65	5	13	.446
66	9	18	.015
67	10	13	.492
68	14	18	.074
69	15	13	.395
70	20	13	.404
71	25	13	.402
72	30	13	.410
73	36	11	.450
74	42	11	.459
75	48	11	.460

Htr	Zone	120 deg	
64	4	18	.606
65	5	14	.757
66	9	18	.600
67	10	14	.807
68	14	18	.661
69	15	14	.701
70	20	14	.711
71	25	14	.709
72	30	14	.717
73	36	12	.566
74	42	12	.576
75	48	12	.577

4.0 TEST DESIGN RATIONALE

4.1 ZONE AND STRIP DESIGNATION

To clearly elucidate the rationale behind the estimation of exchange factors, the nature of an isothermal zone must be understood. As described in section 3.1 , the test article was constructed in the correct geometric shape of the panel and door, but was divided into 48 individually-controlled power zones; each thermally isolated from the others (except by radiation).

Figure 4-1 shows that zones 1 through 15 were those on the top side of the panel simulator, 16 through 30 were on the convex or cavity side of the panel, and zones 31 through 48 were on the door simulator. For purposes of certain calculations, sets of three zones were aggregated into fore-and-aft strips, as shown. For example, strip 1 refers to zones 1, 6, and 11 considered together. Strip 16 is the outboard strip on the door and includes zones 36, 42, and 48.

4.2 HEAT BALANCE EQUATIONS

In order to utilize the test article to experimentally measure zone-to-chamber and zone-to-zone exchange factors the zone temperatures were controlled to limit the energy exchange to desired zones. Thus, by isolating and measuring the energy exchange between particular zones, the normally complex simultaneous equations involving exchange factors can be simplified and solved.

FIGURE 4.1

ZONE AND STRIP NUMBER DESIGNATION

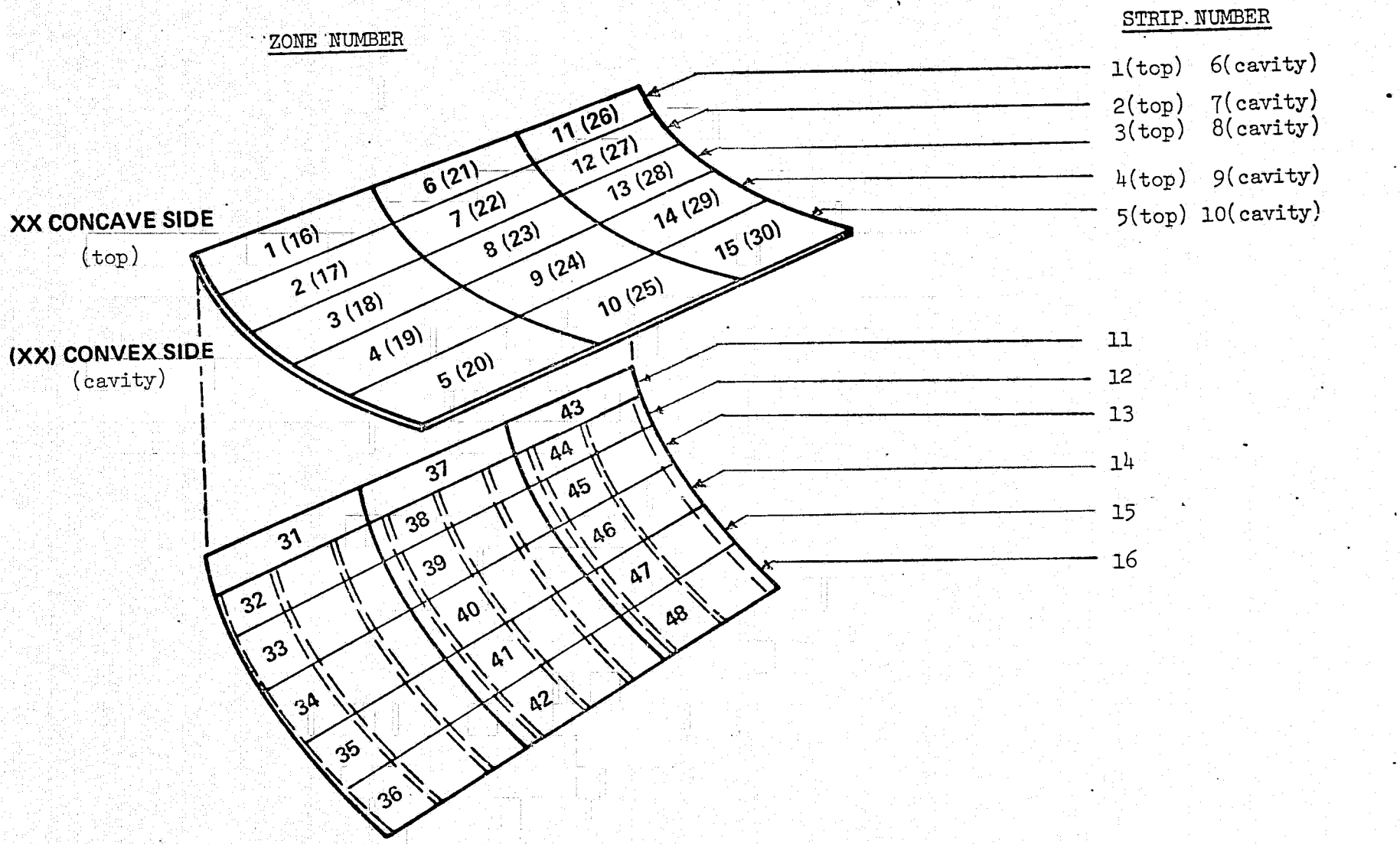

In its general form, the heat balance for the i th zone, which exchanges energy with the chamber, with the solar array mirrors, with all other zones, and receives heat from the "suns" and from its own heater, can be written as follows:

$$Q_i^{sun} + Q_i^{htr} = \sigma E_{i-ch} (T_i^4 - T_{ch}^4) + \sigma E_{i-m} (T_i^4 - T_m^4) + \sum_j E_{i-j} (T_i^4 - T_j^4) \qquad \text{(Eq. 1)}$$

where Q^{sun} = absorbed heat from solar array

Q^{htr} = heater power dissipated in zone i = I^2R

E_{i-ch} = exchangefactor between zone i and chamber

E_{i-m} = exchange factor between zone i and mirrors

E_{i-j} = exchange factor between zones i and j

σ = Stefan-Boltzman constant

T_i, T_j, T_m, T_{ch} = temperature of i th, j th zone, mirror, and chamber

The majority of the testing in Chamber B involved configuring the test article to simplify equation 1 so that certain terms could be experimentally determined.

If the test article is positioned such that the view between the mirror and the cavity is zero (i.e., sun angles $< 20^o$), and if each zone is maintained at the same temperature using the heaters, and the solar lamps are off, Equation 1 becomes:

$$Q_i^{htr} = \sigma E_{i-ch} (T_i^4 - T_{ch}^4) \qquad \text{(Eq. 2)}$$

or

$$E_{i-ch} = \frac{Q_i^{htr}}{\sigma (T_i^4 - T_{ch}^4)}$$

Equation 2 then represents a method of calculating each E_{i-CH} by measuring the power required to maintain each zone at the uniform temperature.

Referring back to Eq. 1, if a particular zone is set to a unique temperature while all other zones are maintained at the same temperature, the following equations result (again, suns are off and mirror is out of sight):

$$Q_i^{htr} = \sigma E_{i-ch} (T_i^4 - T_{ch}^4) + \sigma E_{i-j} (T_i^4 - T_j^4)$$

or

$$E_{i-j} = \frac{Q_i^{htr} - \sigma E_{i-ch} (T_i^4 - T_{ch}^4)}{\sigma (T_i^4 - T_j^4)} \qquad \text{(Eq. 3)}$$

Given that the set of E_{i-CH} have been previously determined using Equation 2, Equation 3 can be used to experimentally determine the full set of zone-to-zone exchange factors. Due to time limitations on the testing, and the fact that experimental inaccuracy tends to mask the smaller exchange factors, only the more significant exchange factors were measured using this method.

A check of the method was available using the exchange factor reciprocity relationship. In terms of Equation 3, this can be stated as:

$$E_{i-j} = E_{j-i} \qquad \text{(Eq. 4)}$$

Thus, by changing the unique zone, it is possible to obtain independently both E_{i-j} and E_{j-i}.

With the solar lamps on, two independent methods of measuring Q^{sun} are available, and the agreement between these methods yields another check on the previously determined exchange factors. Assuming for the moment that the set of exchange factors with the mirror is known, method 1 involves turning the heaters off and allowing each zone to reach equilibrium in the solar beam. Equation 1 becomes:

$$Q_i^{sun} = \sigma E_{i-ch} (T_i^4 - T_{ch}^4) + \sigma E_{i-m} (T_i^4 - T_m^4) + \sum_j E_{i-j} (T_i^4 - T_j^4) \qquad \text{(Eq. 5)}$$

and since all exchange factors are known, the absorbed solar heating on each zone is calculable.

The second method requires using the heaters to maintain a constant temperature in the cavity, which removes the cross terms and reduces Equation 1 to the following form:

$$Q_i^{sun} = \sigma E_{i-ch} (T_i^4 - T_{ch}^4) + \sigma E_{i-m} (T_i^4 - T_m^4) - Q_i^{htr} \qquad \text{(Eq. 6)}$$

For the same sun angle, the value of Q_i^{sun} from Equations 5 and 6 should agree, although the contributions from the various terms will be different.

Several limitations to these methods should be mentioned. First, the accuracy problems become extreme for small values of E_{i-j}. In particular, for the smaller factors, Equation 3 requires the calculation of the difference of two large numbers, each subject to experimental inaccurary. Thus, a small percentage change in either of the two terms

which form the difference can result in a large error in the exchange factor. This fact limited the use of this method to the larger (end, or course, more important) exchange factors.

The discrete nature of the zones limited the testing to sun angles which provided a shadow line at a zone boundary. With the shadow line through a zone, it was deemed impossible to know accurately the average temperature of the zone and to insure that the zones were isothermal.

At the higher sun angles, with the sun shining directly into the cavity, it became impossible to maintain all zones at the same temperature, due to the high equilibrium temperature of certain zones and the power limitation on the heaters. At these angles, only method 1 and Equation 5 could be used for absorbed heat determination.

Equations 2, 3 and 6 were programmed into the real-time test monitoring computer facilities at NASA-JSC, and results were continuously available. The program calculated heater power directly from the power supply current readings, and temperature-dependent resistance curves for each heater, which were provided by the manufacturer and checked before the test began. Test procedures required careful determination that stability had been reached before data was taken. Obviously, all equations developed above are only valid when steady conditions are reached.

5.0 TEST DESCRIPTION

The entire test series encompassed seven weeks of in-chamber test time, organized as follows:

WEEK	DATES	CHAMBER	BRIEF DESCRIPTION
1	3/3-3/7	B	Exchange factors
2	3/10-3/14	B	Absorbed heat
3	3/17-3/21	B	Exchange factors
4	3/24-3/28	B	Wide cavity; white door
5	4/22-4/26	A	QLA calibration; absorbed heat
6	4/29-5/1	A	QLA calibration; absorbed heat
7	6/16-6/20	B	Background

Although the background testing was accomplished last, the results will be described first since they are required to interpret other test data.

5.1 BACKGROUND MEASUREMENT

Table 5-1 describes the test points undertaken during the week of background testing in Chamber B. The basic background measurements were made by scanning the test article (with radiometers attached) through a range of angles and recording flux readings at each angle. Scans were accomplished for various test article conditions in order to evaluate the influence of reflected energy on the test article.

The necessity for this test was due to unanticipated results from weeks 1 through 4, which led to the conclusion that chamber background was non-negligible. Although the chamber walls are black and maintained at

TABLE 5-1

CAVITY BACKGROUND TEST

SUMMARY OF TEST POINTS

TEST POINT	SUN ANGLE (deg)	SUNS ON/OFF	TEMPERATURE (°F)		TIME (DAY, HR, MIN)	
			PANEL	DOOR	START	END
1	20	off	40	Equilb.	167:0154	1247
1A	scan	off	40	↓	1247	1328
2	20	off	80	↓	1330	1900
2A	scan	off	80	↓	1900	1930
3	20	off	120	↓	1930	168:0030
3A	scan	off	120	↓	0030	0100
4	20	off	40	40	0100	0430
4A	scan	off	40	40	0430	0505
5	20	off	80	80	0505	0835
5A	scan	off	80	80	0835	0903
6	20	off	120	120	0903	1230
6A	scan	off	120	120	1230	1300
7	77	off	40	40	1300	1630
8	77	off	80	80	1630	2050
9	77	off	120	120	2050	2345
10	77	on	equilibrium		2345	169:0700
11	77	off	same as T.P. 10		0700	0708
12	77	off	same as T.P. 10		0708	1110
13	103	on	equilibrium		1110	1835
14	103	off	same as T.P. 13		1835	1850
15	103	off	same as T.P. 13		1850	2150
16	131	on	equilibrium		2150	170:0600
17	131	off	same as T.P. 16		0600	0616
18	131	off	same as T.P. 16		0616	1102
18A	131	on	match March test		1102	1436
19	46	on	120	120	1436	2120
20	63	on	120	120	2120	171:0105
20A	63	off	120	120	0105	0120
21	140	on	120	120	0120	0615
21A	scan	on	120	120	0615	0645
21B	140	off	120	120	0645	0725
22	scan	off	cold soak		0725	1400

LN_2 temperatures (generally below -290°F), reflections from the walls was unknown. Further, the solar array mirrors are maintained at 70°F by water circulation and thus provide a source of emitted as well as reflected energy. The results of these background measurements are discussed in Section 6.1.

Other test points were run to confirm exchange factor data previously measured in weeks 1 through 4. Also, additional solar testing was conducted using a method of determining absorbed heat that was designed after the partial failure of earlier absorbed heat measurements.

5.2 CAVITY ASSESSMENT - CHAMBER B

Six distinct types of test points were accomplished during the four weeks of testing, based on various uses of the heat balance equation developed in Section 4.0. Also, a total of five different test article configurations were tested. Table 5-2 describes the six test point types and the five test article configurations.

Table 5-3 lists the test points accomplished and the key conditions set up for each. The codes in the columns entitled "TEST POINT TYPE" and "TEST CONFIGURATION" refer to the descriptions presented in Table 5-2.

5.3 CAVITY ASSESSMENT - CHAMBER A

Table 5-4 lists the test points accomplished during the two weeks of Chamber A cavity assessment. The effect of the QLA and the IR panel on test article performance were evaluated to determine the magnitude of absorbed heat from these sources. Various combinations of lamp settings were tested to calibrate the QLA performance for future testing with a flowing radiator. In addition, exchange factors to space (chamber) were determined.

TABLE 5-2

TEST POINT TYPES AND TEST ARTICLE CONFIGURATIONS DURING CAVITY ASSESSMENT TESTING

TEST POINT TYPE	CONDITION/OBJECTIVES
D	All zones maintained at same temperature - calculate exchange factors to space
E	All zones maintained at same temperature except "unique" zone - calculate exchange factors from each zone to unique zone
B	All zones maintained at same temperature - calculate background flux
S	All zones maintained at same temperature - solar lamps on - calculate heat absorbed by each zone
EQ	All power to zones off - observe equilibrium temperature of each zone
W	No requirement on temperatures - observe heater power settings and temperatures for matrix solution of exchange factors

TEST ARTICLE CONFIGURATION	DESCRIPTION
TB	Teflon-covered door; beams on
TNB	Teflon-covered door; no beams
BNB	Beta cloth-covered door; no beams
BSNB	Beta cloth stripe on door; no beams
TWNB	Teflon-covered door; wide cavity; no beams

TABLE 5-3

CAVITY ASSESSMENT TEST
SUMMARY OF TEST POINTS

TEST POINT	TEST POINT TYPE	TEST CONFIG.	SUN ANGLE	UNIQUE ZONE-TOP	UNIQUE ZONE-CAV.	START TIME	STOP TIME
1	D	TB	-75	---	---	62:1016	62:1644
2	D	TB	20	---	---	62:1644	63:0740
4	E	TB	20	1	16	63:0740	63:1124
5	E	TB	20	9	24	63:1124	63:1535
6T	E	TB	20	2	---	63:1535	63:1757
6C	E	TB	20	---	17	63:1535	63:2000
7	E	TB	20	5	20	63:2000	64:0159
8T	E	TB	20	6	---	64:0159	64:0414
8C	E	TB	20	---	21	64:0159	64:0737
9T	E	TB	20	4	---	64:0414	64:0737
9C	E	TB	20	---	19	64:0737	64:1030
10T	E	TB	20	7	---	64:0737	64:1030
17T	E	TB	20	12	---	64:1030	64:1318
17C	E	TB	20	---	40	64:1030	64:1615
20T	E	TB	20	13	---	64:1318	64:1950
20C	E	TB	20	---	34, 51	64:1615	64:2314
WET-1	W	TB	20	---	---	64:2314	65:0040
WET-2	W	TB	20	---	---	65:0040	65:0235
WET-3	W	TB	20	---	---	65:0235	65:0430
16C	E	TB	20	---	33, 50	64:2231	65:0620
WET-4	W	TB	20	---	---	65:0620	65:0730
15C	E	TB	20	---	32, 49	65:0620	65:0929
WET-5	W	TB	20	---	---	65:0730	65:0920
29	B	TB	77	---	---	65:0920	65:1830
31	B	TB	131	---	---	65:1830	65:2214
40	S	TB	131	---	---	66:0430	66:1330
38	EQ	TB	77	---	---	66:1330	66:1745
			REPRESS			66:1900	
46	EQ	TNB	20	---	---	69:0700	69:1930
47	EQ	TNB	46	---	---	69:2000	70:0120
48	EQ	TNB	63	---	---	70:0130	70:0945
49	EQ	TNB	103	---	---	70:0945	70:1555
50	EQ	TNB	131	---	---	70:1555	71:0115
53	EQ	TNB	77	---	---	71:0115	71:0700
			REPRESS			71:0710	
54	EQ	BNB	20	---	---	71:2200	72:0600
55	EQ	BNB	46	---	---	72:0650	72:1305
56	EQ	BNB	131	---	---	72:1305	72:1705
57	EQ	BNB	63	---	---	72:1705	72:2115
59	EQ	BNB	103	---	---	72:2115	73:0435
58, 61	EQ	BNB	77, 77+	---	---	73:0435	73:0955
			REPRESS			73:1000	
62	D	TNB	20	---	---	76:0532	76:1322
63	E	TNB	20	1	16	76:1322	76:1755
64	E	TNB	20	2	17	76:1755	76:2205
65	E	TNB	20	3	18	76:2205	77:0305
66	E	TNB	20	4	19	77:0305	77:0843
67	E	TNB	20	5	20	77:0843	77:1205

TABLE 5-3 (continued)

TEST POINT	TYPE	TEST CONFIG.	SUN ANGLE	UNIQUE ZONE-TOP	UNIQUE ZONE-CAV.	START TIME	STOP TIME
68	E	TNB	20	7	31	77:1205	77:1835
69	E	TNB	20	8	32	77:1730	77:2105
70	E	TNB	20	10	33	77:2105	77:2355
71	E	TNB	20	11	34	77:2355	78:0330
72	E	TNB	20	12	35	78:0330	78:0912
73	E	TNB	20	14	36	78:0912	78:1315
74	E	TNB	20	15	40	78:1315	78:1750
75	E	TNB	20	13	46	78:1750	78:2255
76	S	TNB	131	---	---	78:2255	79:1015
77	S	TNB	140	---	---	79:1015	79:1800
78	S	TNB	63	---	---	79:1800	80:0310
79	S	TNB	0	---	---	80:0310	80:1024
80	S	TNB	46	---	---	80:1024	80:1800
			REPRESS			80:1851	
90	EQ	BSNB	77,77+	---	---	83:0546	83:0930
91	EQ	BSNB	103	---	---	83:0930	83:1230
92	EQ	BSNB	131	---	---	83:1230	83:1730
			REPRESS			83:1730	
93	D	TWNB	52	---	---	84:0700	84:1600
94	E	TWNB	52	---	16	84:1600	84:2110
95	E	TWNB	52	---	17	84:2110	85:0205
96	E	TWNB	52	---	18	85:0205	85:0600
97	E	TWNB	52	---	19	85:0600	85:0940
99	E	TWNB	52	---	31	85:0940	85:1400
100	E	TWNB	52	---	32	85:1400	85:1815
101	E	TWNB	52	---	33	85:1815	85:2220
102	E	TWNB	52	---	34	85:2220	86:0011
103	E	TWNB	52	---	35	86:0011	86:0232
98	E	TWNB	52	---	20	86:0232	86:0407
104	S	TWNB	52	---	---	86:0413	86:1015
108	S	TWNB	66.5	---	---	86:1015	86:1714
105	S	TWNB	148.5	---	---	86:1714	86:2325
106	S	TWNB	119	---	---	86:2325	87:0536
107	EQ	TWNB	81	---	---	87:0536	87:1230
109	EQ	TWNB	88	---	---	87:1230	87:1445
110	EQ	TWNB	115	---	---	87:1445	87:1710
111	E	TWNB	166	---	---	87:1710	87:1955
			REPRESS			87:2000	

TABLE 5-4

CHAMBER A

CAVITY ASSESSMENT TEST

SUMMARY OF TEST POINTS

TEST POINT	START TIME	STOP TIME	CONDITIONS					
			CAV TEMP	IR PANEL TEMP	TOP TEMP	LAMPS ON	LAMP SETTING	OBJECTIVE
112	APR 22 112:1145	113:1530	40	40	40	OFF	OFF	No Flux
113	113:1530	114:0805	40	20	40	ALL	15	↑
114	114:0805	114:1450	40	0	40	ALL	30	↑
115	114:1450	115:0000	40	-20	40	ALL	45	Constant
116	115:0000	116:0315	40	-40	40	ALL	60	Flux
117	116:0315	116:0820	40	-60	120	ALL	75	↓
118	116:0820	116:0945	40	-80	120	ALL	90	↓
119	116:0945	APR 26 116:1255	NO	DATA	120	ALL	105	↓
REPRESS	116:2130							
120	APR 29 119:2130	119:0440	120	40	120	ALL	120	↓
121	119:0440	119:1056	120	20	120	ALL	135	↓
126	119:1056	119:1345	120	0	120		FULL	SKEWED
122	119:1345	119:1703	120		140	9,8	FULL	FLUX
123	119:1703	119:2130	120	-20	140	9,8,7	FULL	↓
124	119:2130	120:0020	NO	DATA		9,8,7,6	FULL	↓
REPRESS	120:0100							
125	121:0900	121:1208	40	0	180	9,8,7,6,5,4	FULL	↓
127	121:1208	121:1325	100	0	180	9,8,7,6,5,4	FULL	TEST HEAT LEAK
128	121:1325	121:1421	TRANS	0	TRANS	OFF	OFF	TEST SYMMETRY
129	121:1421		CONSTANT CURRENT	0	CONSTANT CURRENT	OFF	OFF	TEST SYMMETRY
REPRESS								

6.0 TEST RESULTS

6.1 BACKGROUND ENVIRONMENT

The results obtained by scanning the test article through a range of angles provided chamber background fluxes for use in subsequent calculations. Appendix A contains the plotted environment data for each radiometer.

Four of the scan test points were accomplished with approximately constant panel and door temperatures. The average flux recorded by the eight cavity radiometers is given in Table 6-1 for each of the four temperatures and eight key cavity-sun angles. By comparing the flux values as a function of temperature, the relative importance of reflections and mirror emission can be deduced.

The top half of Figure 6-1 shows the data plotted against a measure of cavity emission σT^4. A least-squares curve fit to each set of four data points is shown in Figure 6-1 and tabulated in Table 6-1. The slope of the curve is a measure of the component of the flux emitted by the cavity and reflected back onto the radiometer by the mirror. The intercept of each curve represents the flux emitted by the mirrors and incident on the radiometers.

A single heat balance on the cavity can be used to calculate the form factor between the mirror and the cavity, F_{m-c}. In particular, the flux incident on the cavity which was emitted by the mirrors being held at a constant T_m is as follows:

$$q_E = F_{M-C} A_M \sigma \epsilon_M T_M^4 / A_C$$

TABLE 6-1

AVERAGE FLUX AT THE CAVITY PLANE AND RESULTS OF CALCULATION OF FORM FACTOR BETWEEN MIRROR AND CAVITY

SUN ANGLE	AVG. RADIOMETER READING BTU/HR/FT² PANEL/DOOR TEMPERATURE				RESULT OF LEAST SQUARES CURVEFIT		APPROXIMATION OF MIRROR-TO-CAVITY FORM FACTOR	
	-150°F	40°F	80°F	120°F	INTERCEPT	SLOPE	INTERCEPT METHOD	SLOPE METHOD
20	.63	1.63	1.63	2.07	.57	7.88 E-3	.013	.090
46	4.88	7.38	6.81	7.06	5.12	1.22 E-2	.115	.112
63	7.79	11.94	12.31	13.50	7.67	3.22 E-2	.172	.182
77	10.44	15.13	16.56	16.25	10.54	3.51 E-2	.237	.190
103	11.31	15.75	16.25	18.63	10.85	4.01 E-2	.244	.203
120	9.94	14.19	14.83	17.56	9.33	4.16 E-2	.210	.206
131	8.13	13.06	12.94	14.75	8.01	3.65 E-2	.180	.194
140	6.06	11.25	11.13	12.88	5.98	3.76 E-2	.134	.197

FIGURE 6-1 RESULTS OF BACKGROUND TESTING (SOLAR OFF)

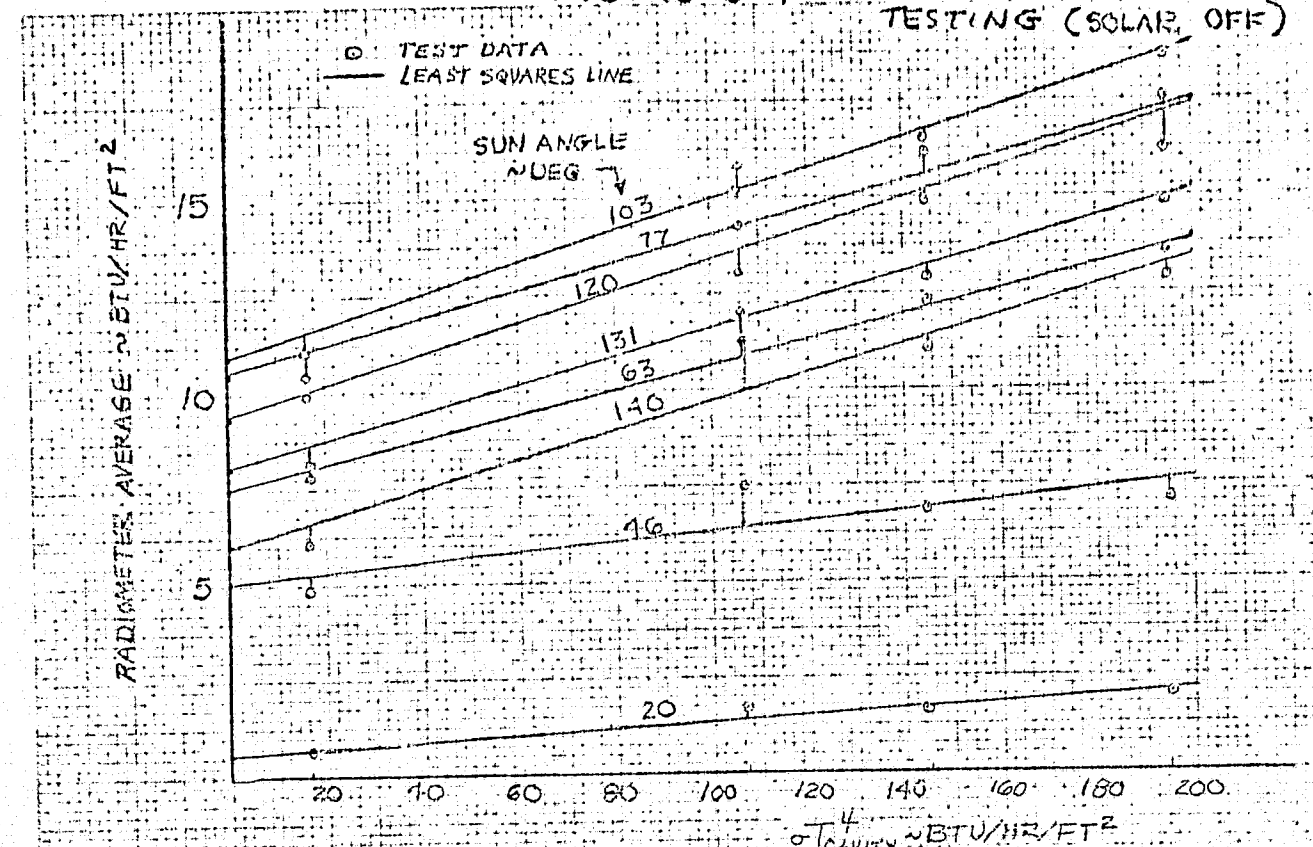

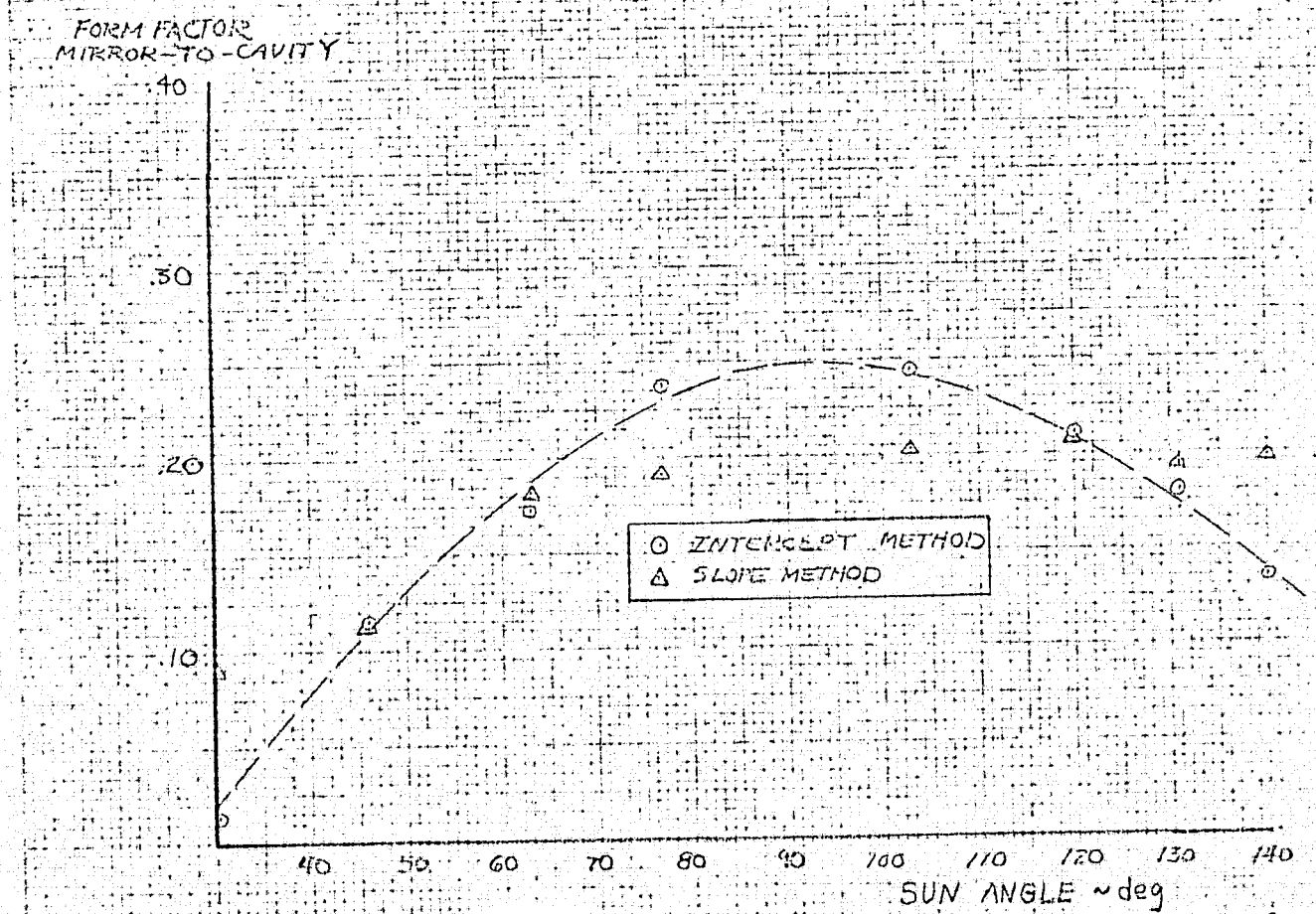

The heat emitted by the cavity at T_c and reflected back onto the radiometers is:

$$q_R = F_{M-C}\,(1-\epsilon_M)\,F_{C-M}\,A_C\,\epsilon_C\,\sigma T_C^4 / A_C$$

$$q_R = F_{M-C}^2\,\frac{A_M}{A_C}\,(1-\epsilon_M)\,\epsilon_C\,\sigma T_C^4$$

And the total flux on the radiometers $q_T = q_E + q_R$ is given by:

$$q_T = F_{M-C}\,\frac{A_m}{A_C}\,\epsilon_M\,\sigma T_M^4 + F_{M-C}^2\,\frac{A_M}{A_C}\,(1-\epsilon_M)\,\epsilon_C\,\sigma T_C^4$$

$$q_T = \text{INTERCEPT} + \text{SLOPE}\,(\sigma T_C^4)$$

Thus, both intercept and slope can be used to calculate F_{m-c}, as follows:

$$F_{M-C} = \frac{\text{INTERCEPT} \cdot A_C}{A_m \epsilon_M \sigma T_M^4}$$

$$F_{M-C} = \sqrt{\frac{\text{SLOPE} \cdot A_C}{A_M (1-\epsilon_M)\,\epsilon_C}}$$

The results of these calculations are plotted in the lower half of Figure 6-1 and tabulated in Table 6-1. The mirror emissivity, ϵm was taken to equal .2, and the cavity emissivity, ϵc was taken to equal .76.

An analysis of the data was also made to determine the existance of any fore-and-aft asymetries in the background flux. Table 6-2 displays the results of averaging the three radiometers on the left side of the cavity (ZF6023, 24, 25) and comparing this with a similar right side average (ZF6027, 28, 29). The difference between these two averages was studied and found to be not significantly different from a normally distributed error term indicative of a random variation. Thus, the existence of a systematic environmental bias was rejected.

TABLE G-2
COMPARISON OF FLUX READINGS ON LEFT AND RIGHT SIDE OF CAVITY

BTU/HR/FT^2

SUN ANGLE (deg)	DATA COMPILATION	PANEL/DOOR TEMPERATURE −150°F	40°F	80°F	120°F
20	LEFTSIDE AVG +	0	2.0	1.0	2
	RIGHTSIDE AVG ++	1.0	1.7	2.0	2.1
	DIFFERENCE	+1.0	−0.3	+1.0	+0.1
46	LEFTSIDE AVG	5.0	8.2	6.8	7.3
	RIGHTSIDE AVG	5.7	7.0	6.8	6.7
	DIFFERENCE	+0.7	−1.2	−	−0.6
63	LEFTSIDE AVG	7.5	11.3	12.5	12.3
	RIGHTSIDE AVG	8.7	11.7	11.0	12.7
	DIFFERENCE	+1.2	+0.4	−1.5	+0.4
77	LEFTSIDE AVG	9.8	14.5	15.8	15.8
	RIGHTSIDE AVG	11.0	15.0	15.8	15.8
	DIFFERENCE	+1.2	+0.5	−	−
103	LEFTSIDE AVG	11.3	16.0	16.3	19.2
	RIGHTSIDE AVG	11.8	15.2	15.8	17.5
	DIFFERENCE	+0.5	−0.8	−0.5	−1.7
120	LEFTSIDE AVG	10.2	14.0	15.0	17.3
	RIGHTSIDE AVG	10.0	14.2	13.8	16.8
	DIFFERENCE	−0.2	+0.2	−1.2	−0.5
131	LEFTSIDE AVG.	7.8	13.3	12.8	14.5
	RIGHTSIDE AVG.	8.8	12.2	12.2	13.5
	DIFFERENCE	+1.0	−1.1	−0.6	−1.0
140	LEFTSIDE AVG	7.3	11.3	11.0	12.0
	RIGHTSIDE AVG	7.3	11.0	11.0	13.0
	DIFFERENCE	-	−0.3	−	+1.0

\+ avg of ZF6023, 24, 25

++ avg of ZF6027, 28, 29

MEAN DIFFERENCE = −.0438 °F ($\bar{\mu}$)

MEDIAN DIFFERENCE = 0.0 °F

SAMPLE VARIANCE = .7007 °F ($\bar{\sigma}^2$)

$t = (\bar{\mu} - 0)/(\bar{\sigma}^2/\sqrt{n}) = -.3536$

6.2 EXCHANGE FACTORS TO SPACE

Tables 6-3, 6-4, and 6-5 display the test results from all test points conducted to determine individual zone exchange factors to space. The three tables include data pertaining to the panel top side, panel bottom side, and door, respectively.

As described in Section 4.2, the exchange factors were calculated automatically by the on-line computation facilities. The equation used in the calculation was:

$$\mathcal{F}_{i\rightarrow ch} = \frac{Q_i^{htr}}{\sigma A_i (T_i^4 - T_{ch}^4)}$$

Where Q, A, and T refer to heater power, area, and temperature, respectively. The value of T_{ch}, the chamber wall temperature, was input to the computer based on wall-mounted thermocouples, and was in the range -290°F to -305°F throughout the test series.

Exchange factors between the cavity zones and space (Tables 6-4 and 6-5) were calculated on five different occassions; once with the beams in place and four times with beams removed. Comparison is made between these calculations and analytical predictions made with the M-TRAP computer routine.

Table 6-6 aggregates the data shown in the previous three tables into the "strip" form as described in Section 4.1. The data exhibits a high degree of stability over the five test points, especially given the 3 month time interval between the March and June tests, during which time the test article was moved, disconnected, subjected to an intervening test in Chamber A, and inadvertently doused with water during a malfunction of

TABLE 6-3

EXCHANGE FACTORS TO SPACE

TOP OF RADIATOR

ZONE	AREA, (FT^2)	DIFFUSE PREDICTION $\mathcal{F}$	$\mathcal{F}_{MEASURED}$	$\mathcal{F}_A$
1	6.60	.678	.566	
2	5.11	.713	.595	3.04
3	9.23	.744	.651	6.01
4	13.74	.760	.674	9.26
5	18.32	.768	.679	12.44
6	6.60	.656	.561	3.70
7	5.11	.700	.689	3.52
8	9.23	.737	.640	5.91
9	13.74	.753	.657	9.03
10	18.32	.761	.668	12.24
11	6.60	.679	.642	4.24
12	5.11	.715	.660	3.37
13	9.23	.744	.653	6.03
14	13.74	.760	.687	9.44
15	18.32	.768	.645	14.07

TABLE 6-4

TEST RESULTS - EXCHANGE FACTORS TO SPACE-PANEL

ZONE	AREA (ft^2)	TEST POINT 2 MARCH, BEAMS ON ALL ZONES 40° F_s	F_sA	TEST POINT 62 MARCH, BEAMS OFF ALL ZONES 40° F_s	F_sA	TEST POINT 4 JUNE, BEAMS OFF ALL ZONES 40° F_s	F_sA	TEST POINT 5 JUNE, BEAMS OFF ALL ZONES 80°F F_s	F_sA	TEST POINT 6 JUNE, BEAMS OFF ALL ZONES 120°F F_s	F_sA
16	6.6	.169	1.12	.188	1.241	.144	.95	.155	1.023	.155	1.023
17	5.35	.122	0.65	.137	.732	.124	.663	.135	.722	.130	.696
18	9.35	.219	2.05	.234	2.19	.207	1.94	.212	1.98	.210	1.96
19	13.84	.370	5.12	.381	5.27	.356	4.92	.369	5.11	.371	5.13
20	18.46	.610	11.26	.606	11.19	.576	10.63	.576	10.63	.590	10.89
Subtotal			20.20		20.62		19.10		19.47		19.70
21	6.6	.0936	0.62	.107	.706	.099	0.65	.104	.687	.142	.937
22	5.35	.074	0.40	.081	.430	.043	0.23	.054	.289	.058	.310
23	9.35	.138	1.29	.141	1.32	.116	1.08	.127	1.19	.132	1.23
24	13.84	.310	4.29	.310	4.29	.287	3.97	.300	4.15	.306	4.24
25	18.46	.585	10.80	.585	10.80	.563	10.39	.564	10.41	.569	10.50
Subtotal			17.40		17.55		16.32		16.73		17.22
26	6.6	.124	0.82	.124	.818	.133	.878	.145	.957	.146	.964
27	5.35	.136	0.73	.164	.877	.153	.808	.172	.920	.176	.942
28	9.35	.221	2.07	.234	2.19	.206	1.93	.228	2.13	.234	2.19
29	13.84	.406	5.62	.399	5.52	.383	5.30	.386	5.34	.380	5.38
30	18.46	.626	11.56	.624	11.52	.606	11.19	.606	11.18	.613	11.32
Subtotal			20.80		20.93		20.11		20.53		20.80
Panel Total	160.8		58.40		59.09		55.53		56.72		57.71
Door Total *	181.38		61.41		57.45		57.75		58.32		58.58
Grand Total	342.18		119.81		116.54		113.28		115.04		116.29

* See Table 3

TABLE 6-5

TEST RESULTS - EXCHANGE FACTORS TO SPACE-DOOR

ZONE	AREA (ft^2)	TEST POINT 2 MARCH, BEAMS ON ALL ZONES 40° F_s	F_sA	TEST POINT 62 MARCH, BEAMS OFF ALL ZONES 40° F_s	F_sA	TEST POINT 4 JUNE, BEAMS OFF ALL ZONES 40° F_s	F_sA	TEST POINT 5 JUNE, BEAMS OFF ALL ZONES 80°F F_s	F_sA	TEST POINT 6 JUNE, BEAMS OFF ALL ZONES 120°F F_s	F_sA
31	4.13	.246	1.02	.241	.995	.262	1.082	.280	1.16	.276	1.14
32	5.30	.359	1.90	.263	1.39	.27	1.43	.277	1.47	.274	1.45
33	6.72	.321	2.16	.32	2.15	.322	2.16	.323	2.17	.323	2.17
34	10.12	.320	3.24	.293	2.97	.327	3.31	.328	3.32	.324	3.28
35	14.34	.377	5.41	.336	4.82	.335	4.80	.338	4.85	.337	4.83
36	19.85	.427	8.48	.390	7.74	.402	7.98	.403	8.00	.409	8.12
Subtotal			22.21		20.07		20.76		20.97		20.99
37	4.13	.186	0.77	.175	.723	.192	.793	.214	0.88	.203	0.84
38	5.30	.254	1.35	.180	.954	.179	.949	.187	0.99	.181	0.96
39	6.72	.262	1.76	.280	1.88	.273	1.83	.270	1.81	.268	1.80
40	10.12	.263	2.66	.261	2.64	.259	2.62	.261	2.64	.262	2.65
41	14.34	.280	4.02	.274	3.93	.279	4.00	.283	4.06	.284	4.07
42	19.85	.338	6.71	.331	6.57	.322	6.39	.331	6.57	.335	6.65
Subtotal			17.27		16.70		16.58		16.95		16.97
43	4.13	.222	0.92	.259	1.07	.255	1.05	.269	1.11	.261	1.08
44	5.30	.357	1.89	.253	1.34	.248	1.314	.248	1.31	.247	1.31
45	6.72	.354	2.38	.355	2.39	.331	2.22	.334	2.24	.335	2.25
46	10.12	.360	3.64	.348	3.52	.356	3.60	.331	3.35	.335	3.39
47	14.34	.367	5.26	.348	4.99	.34	4.87	.344	4.93	.344	4.93
48	19.85	.395	7.84	.372	7.38	.371	7.36	.376	7.46	.386	7.66
Subtotal			21.93		20.69		20.41		20.40		20.62
Door Total	181.38		61.41		57.45		57.75		58.32		58.58

TABLE G-G
EXCHANGE FACTORS TO SPACE

STRIP MODEL
(ft^2)

	STRIP NUMBER	AREA (ft^2)	EXCHANGE FACTOR TO CHAMBER ~ ft^2						WIDE CAVITY	
			DIFFUSE PREDICTION $\epsilon = .8$	TEST PT. 2	TEST PT. G2	TEST PT. 4	TEST PT. 5	TEST PT. 6	EXCHANGE FACTOR TO CHAMBER ~ ft^2	% INCREASE OVER B/L CAVITY
PANEL TOP	1	19.80	13.27	11.68						
	2	15.33	10.86	9.93						
	3	27.69	20.54	17.95						
	4	41.22	31.23	27.73						
	5	54.96	42.08	38.75						
	SUB TOTAL	159.00	117.98	106.04						
PANEL BOTTOM	6	19.80	2.50	2.56	2.76	2.48	2.67	2.92	3.74	35.0
	7	16.05	2.69	1.78	2.34	1.70	1.93	1.95	3.01	28.5
	8	28.05	7.20	5.41	5.70	4.95	5.30	5.38	9.21	61.6
	9	41.52	17.49	15.03	15.08	14.19	14.60	14.75	21.08	39.7
	10	55.38	36.30	33.62	33.51	32.21	32.22	32.71	36.32	8.3
	SUB TOTAL	160.80	66.18	58.40	59.39	55.53	56.72	57.71	73.36	25.6
	RADIATOR TOTAL	319.80	184.16	164.44	165.43	161.96	162.76	163.75	179.40	9.0
PAYLOAD BAY DOOR	11	12.39	1.79	2.71	2.79	2.93	3.15	3.06	3.64	34.3
	12	15.90	5.36	5.14	3.68	3.69	3.77	3.72	4.75	29.0
	13	20.16	7.06	6.30	6.42	6.21	6.22	6.22	7.69	19.7
	14	30.36	10.70	9.54	9.13	9.53	9.31	9.32	11.38	24.6
	15	43.02	16.29	14.69	13.74	13.67	13.84	13.83	16.42	19.5
	16	59.55	26.28	23.03	21.69	21.73	22.03	22.43	25.21	16.2
	DOOR TOTAL	181.38	67.48	61.41	57.45	57.76	58.32	58.58	69.09	20.2

the automatic fire suppression equipment in Chamber A.

With beams off, the range of exchange factor totals is well within the range of experimental accuracy to be expected from the test equipment, thus, increasing the confidence in the validity of the results. The results obtained with the beams in place are within the accuracy tolerance for the equipment, resulting in a conclusion that the presence or absence of the beams produces insignificant differences.

Figure 6-2 displays the strip-aggregated data of Table 6-6 in graphical form, demonstrating the close agreement between test and analysis. With an assumed IR emissivity of ε=.72, the computer predictions are almost identical to the test results, further increasing confidence in the test procedure and the diffuse assumption involved in the computer simulation.

From Table 6-6, test points 4, 5, and 6, it can also be seen that the total exchange factor to space increases with the temperature of the test article. In particular, raising the test article temperature from $40^{\circ}F$ to $120^{\circ}F$, a 16% increase in absolute temperature, raises the measured exchange factor from the panel underside to space from 55.53 ft^2 to 57.71 ft^2, a 4% increase. This phenomenon is assumed to be due to slowly changing material properties with temperature, although the change is small enough to be safely ignored.

6.3 EXCHANGE FACTORS - ZONE TO ZONE

Table 6-7 displays the results of zone-to-zone exchange factor determination for those factors large enough to be amenable to this type of analysis. The results show the determination of a particular exchange factor

FIGURE 6-2
EXCHANGE FACTORS
TO SPACE

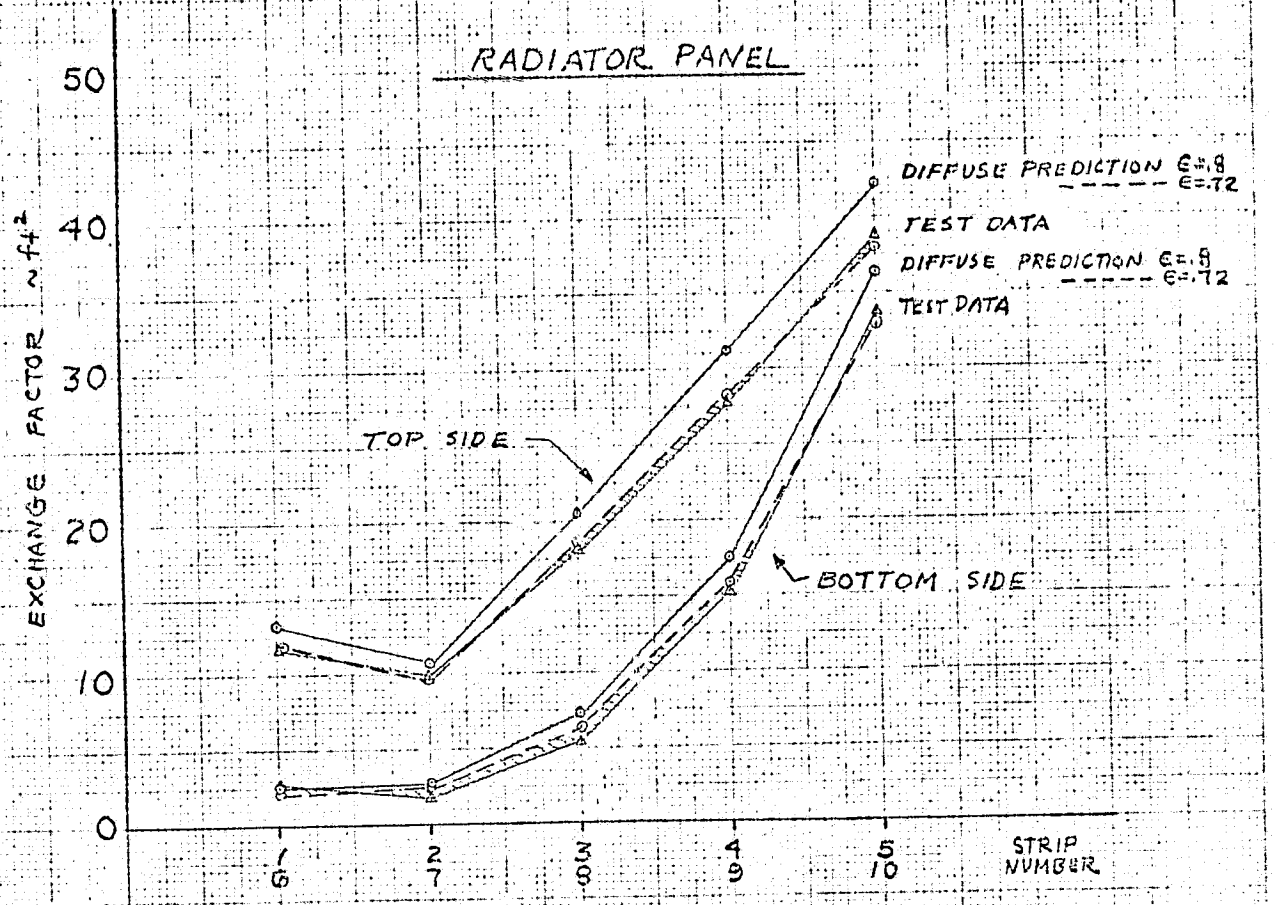

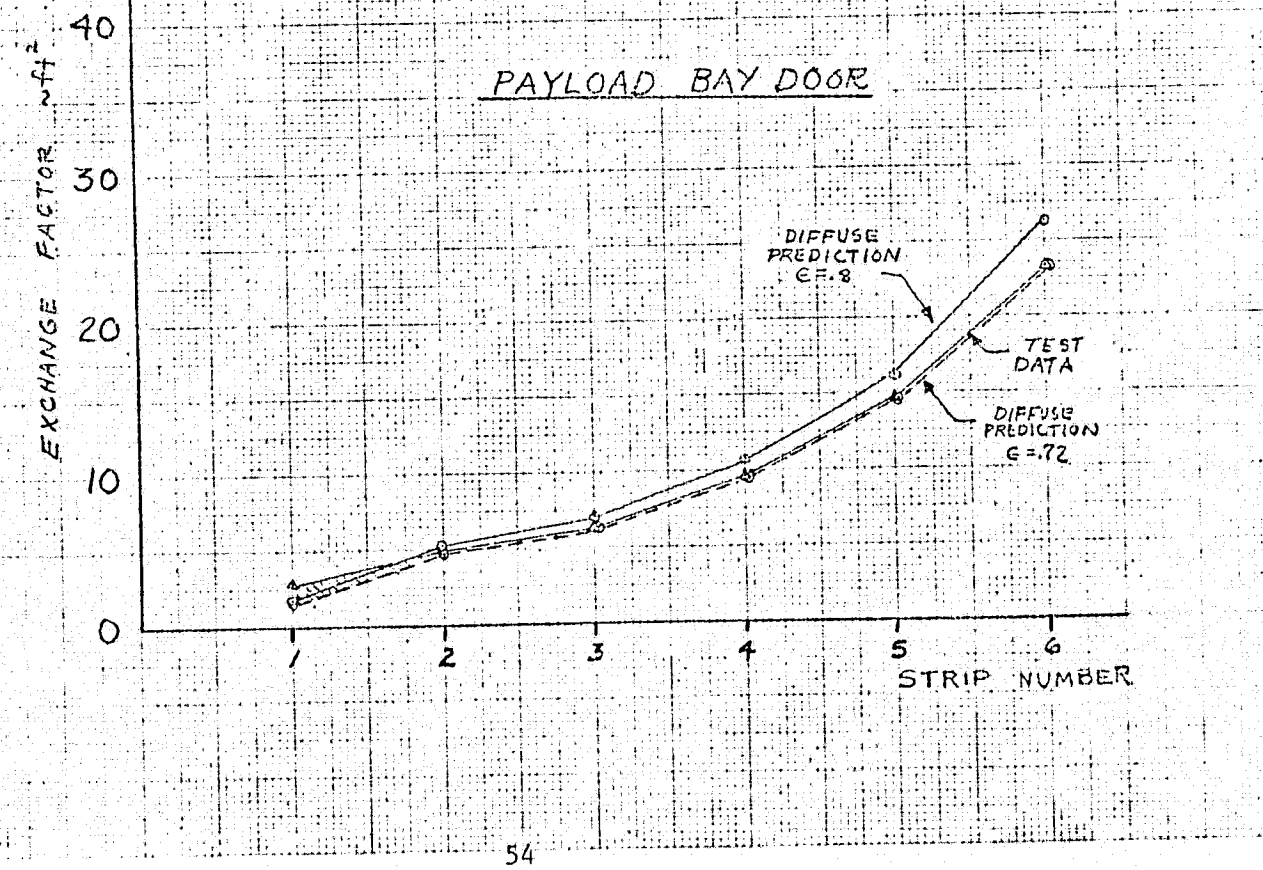

TABLE 6-7

TEST RESULTS--EXCHANGE FACTORS BETWEEN ZONES

ooo(xxx) where ooo taken with panel zone "unique"
xxx taken with door zone "unique"

Zone	Zone 31	Zone 32	Zone 33	Zone 34	Zone 35	Zone 36
16	1.54 (1.56)	0.91 (0.67)	0.94 (0.94)	0.43 (0.59)		
17		0.31 (0.30)	0.76 (0.53)	0.97 (0.88)	0.38 (0.38)	
18			0.31 (0.13)	0.96 (1.02)	1.62 (1.71)	0.56 (0.64)
19				0.26 (0.22)	1.28 (1.13)	2.07 (1.91)
20					0.22 (0.08)	0.90 (1.23)

accomplished two ways; by setting a panel zone to the "unique" temperature, and by setting the door zone to the "unique" temperature. The results generally demonstrated reciprocity in the exchange factors to the limitations set by the accuracy of the instrumentation. Exceptions are attributed to experimental inaccuracies although it should be noted that reciprocity is valid only for diffuse emission and it is possible that the silver/Teflon has a reduced emission at low angles.

To further develop the exchange factors between zones, the model of the test article was utilized as discussed in Section 4.1. The advantages of this procedure were (1) simplicity in handling the cross-terms in Equation 5, and (2) elimination of fore-and-aft asymetrics associated with the positioning of the test article in the chamber.

For the types of environments available with this test setup, only lateral (this is hinge line to outboard edge) variations are theoretically possible, and any fore-and-aft irregularities must be due to experimental factors. Table 6-8 shows the final exchange factor matrix, where analytical values based on a diffuse assumption are used where test data was unobtainable. The last row on the table gives the experimentally-determined exchange factors for each strip as a percentage of the sum of that strip's exchange factors.

The sum of all exchange factors for all strips is 255 ft^2, from which an average emittance can be calculated as follows:

$$\epsilon = \frac{\sum_{\text{all zones}} E_{i-j}}{\sum_{\text{all zones}} A_i} = \frac{255}{336.9} = .757$$

TABLE 6-8

TEST RESULTS--EXCHANGE FACTOR MATRIX
(underlined factors were analytically determined)

	6	7	8	9	10	11	12	13	14	15	16
To Chamber	2.77	2.04	5.20	15.08	33.51	2.79	3.68	6.43	9.13	13.74	21.69
6		.25	.12	.04	.01	4.86	2.46	3.26	2.14	.42	.08
7	.25		.26	.11	.03	.22	1.09	2.72	3.46	1.54	.40
8	.12	.26		.40	.15	.05	.05	.90	3.82	6.50	2.76
9	.04	.11	.40		.29	.04	.04	.06	1.11	5.36	8.60
10	.01	.03	.15	.29		.09	.08	.11	.12	1.08	5.82
11	4.86	.22	.05	.04	.09		.23	.20	.35	.42	.42
12	2.46	1.09	.05	.04	.08	.23		.65	.82	.64	.54
13	3.26	2.72	.90	.06	.11	.20	.65		.74	.64	.59
14	2.14	3.46	3.82	1.11	.12	.35	.82	.74		.63	.60
15	.42	1.54	6.50	5.36	1.08	.42	.64	.64	.63		.85
16	.08	.40	2.76	8.60	5.82	.42	.54	.59	.60	.85	
Total	16.41	12.12	20.71	31.13	41.29	9.67	10.28	16.30	22.92	31.82	42.35
% By Test	94	89	91	97	98	79	70	82	86	89	92

The overall panel-to-door exchange factor may be determined by summing elements in Table 6-8 as follows:

$$E_{P-D} = \sum_{i=6}^{10} \sum_{j=11}^{16} E_{i-j}$$

where $E_{i,j}$ is the i-jth element in the symetrical exchange factor matrix given in Table 6-8. The result of this summation gives a panel-to-door exchange factor of 59.24 ft^2.

6.4 ABSORBED HEAT

Absorbed heat data was gathered by the use of two calculational methods, as described in section 4.2. Briefly recapitulating, in Method 1, the test article was allowed to come to equilibrium in the solar beam with all heaters off. Absorbed heat was calculated via a heat balance which required knowledge of all zone-to-zone exchange factors.

Method 2 was used when the test article could be held at the same temperature by using the heaters. This could not be accomplished at high sun angles due to the high equilibrium temperatures for some zones. Method 2 is preferable to Method 1 since it does not require use of the zone-to-zone exchange factors.

Table 6-9 contains temperature and power data for the 11 test points applicable to absorbed heat calculation. Table 6-10 contains aggragated data for the same test points. Total power has been calculated along with area-weighted average temperature.

Figure 6-3 displays equilibrium temperatures (i.e., power-off, area-weighted average temperature) for those test points conducted in this manner. It can

TABLE 6-9

SELECTED TEST DATA

	ZONE	79(0°)		47 (46°)		80(46°)		48(63°)		78(63°)		53(77°)		49(103°)		40(131°)		50(131°)		76(131°)		77(140°)	
		TEMP °F	POWER BTU/hr	TEMP °F	POWER BTU/hr	TEMP °F	POWER BTU/hr	TEMP °F	POWER BTU/hr	TEMP °F	POWER BTU/hr	TEMP °F	POWER BTU/hr	TEMP °F	POWER BTU/hr	TEMP °F	POWER BTU/hr	TEMP °F	POWER BTU/hr	TEMP °F	POWER BTU/hr	TEMP °F	POWER BTU/hr
PANEL TOPSIDE	1	119.7	510	59.6	0	118.9	250	46.9	0	120.1	330	86.0	330	0.0	255	119.3	150	-7.7	255	121.9	750	120.3	730
	2	120.6	330	42.7	0	119.5	270	42.6	0	118.9	290	44.4	250	-9.6	195	120.2	550	-8.4	195	118.0	600	120.2	600
	3	120.6	710	-25.1	0	119.9	900	-46.8	0	119.5	960	3.2	425	-1.3	425	122.1	1180	-0.6	425	119.7	1140	120.3	1120
	4	118.7	890	-33.8	0	119.9	1311	-70.3	0	118.5	1600	-5.8	590	-9.0	590	120.8	1930	-8.3	590	119.5	1740	119.5	1700
	5	120.1	1490	-66.7	0	119.5	1890	-121.7	0	120.6	2410	3.8	865	-5.1	865	120.8	2450	-3.9	865	119.7	2410	121.0	2370
	6	119.5	510	60.5	0	118.8	260	49.6	0	118.9	300	81.7	275	-1.0	245	121.5	770	-10.6	245	119.1	750	120.3	710
	7	119.5	440	31.1	0	118.9	390	34.8	0	120.2	380	46.3	250	1.9	230	121.9	680	-2.6	230	120.2	680	119.3	640
	8	119.5	710	-17.6	0	120.6	880	-37.9	0	120.8	960	5.7	400	3.8	400	121.0	1140	-0.6	400	121.0	1100	120.2	1040
	9	120.7	940	-27.8	0	118.4	1290	-65.3	0	119.3	1570	3.8	625	3.8	625	120.7	1710	0.0	625	121.2	1640	118.7	1590
	10	119.1	1570	-65.3	0	119.0	1910	-117.7	0	120.1	2400	1.9	825	-3.2	825	119.9	2360	-1.9	825	122.1	2340	119.2	2240
	11	119.7	580	37.8	0	119.5	340	40.2	0	118.8	360	83.7	335	13.4	285	120.1	810	-1.9	285	120.1	790	119.1	770
	12	111.5	420	14.0	0	119.9	330	43.2	0	120.3	350	57.2	264	15.9	240	120.3	620	5.7	235	120.8	620	120.7	600
	13	120.5	660	-24.9	0	120.4	810	-23.7	0	119.5	910	17.2	440	21.0	455	120.1	1040	9.5	435	121.0	1080	8.9	1030
	14	120.9	1020	-35.9	0	119.8	1410	-66.4	0	120.1	1650	-2.9	580	-2.9	580	122.6	1790	-5.8	580	119.6	1690	119.6	1640
	15	119.0	1430	-54.5	0	119.5	1870	-117.0	0	121.2	2310	8.6	825	4.8	820	120.9	2290	5.8	820	119.0	2230	119.8	2150
PANEL BOTTOMSIDE	16	45.7	170	-91.5	0	39.8	120	28.5	0	84.5	100	186.0	0	108.2	0	121.9	190	-44.1	0	121.9	200	119.5	210
	17	35.4	50	-68.9	0	38.6	50	98.6	0	124.9	0	112.7	0	98.6	0	120.6	40	3.2	0	122.5	50	120.6	130
	18	39.1	270	-11.7	0	38.7	10	117.2	0	130.5	0	43.2	0	50.5	0	121.7	50	34.6	0	122.1	0	121.9	400
	19	34.2	500	-2.6	0	40.8	160	-19.0	0	100.3	840	-19.0	0	36.5	0	120.6	310	39.6	0	121.2	220	121.9	240
	20	35.4	1300	-112.3	0	39.8	1020	-104.2	0	114.8	2010	-57.7	0	7.7	0	120.1	1080	26.8	0	121.0	970	121.6	890
	21	39.4	70	-75.0	0	39.4	60	52.3	0	101.1	80	219.9	0	138.1	0	122.3	80	-19.6	0	121.6	90	20.1	100
	22	40.8	40	-52.3	0	40.2	30	99.7	0	131.1	0	131.5	0	117.9	0	123.8	0	21.0	0	126.6	0	119.9	80
	23	30.2	70	8.9	0	48.8	0	128.3	0	145.4	0	75.1	0	81.9	0	134.1	0	56.6	0	137.5	0	120.4	120
	24	41.6	460	0.0	0	40.2	130	1.3	0	99.0	620	7.6	0	62.6	0	121.9	80	62.6	0	122.5	0	121.9	10
	25	44.5	1320	-102.2	0	40.0	980	-93.0	0	114.0	1960	-50.8	0	7.7	0	119.5	1210	21.1	0	121.2	1060	120.1	1010
	26	37.9	80	-82.6	0	40.4	70	49.9	0	92.1	60	212.8	0	128.3	0	117.6	100	-37.2	0	120.2	140	120.0	150
	27	40.9	100	-56.6	0	41.0	60	113.5	0	141.8	10	126.6	0	114.3	0	122.3	30	16.3	0	125.2	10	114.5	140
	28	35.6	230	11.5	0	48.2	0	94.6	0	106.8	20	53.5	0	48.7	0	121.4	100	26.7	0	120.6	140	121.0	410
	29	34.4	520	-8.3	0	41.0	240	-16.3	0	103.4	930	-8.4	0	44.5	0	122.1	280	49.3	0	121.0	280	121.2	270
	30	37.1	1330	-111.5	0	39.2	1070	-103.8	0	115.9	2070	-57.3	0	-3.2	0	121.6	1350	7.0	0	121.8	1250	120.5	1190
PAYLOAD BAY DOOR	31	36.3	40	-86.3	0	39.0	90	27.9	0	83.3	40	168.7	0	90.6	0	118.7	170	-39.2	0	122.5	170	121.0	150
	32	42.5	170	-89.2	0	38.4	130	21.6	0	74.1	40	127.7	0	100.9	0	119.6	210	-37.2	0	121.6	250	120.4	260
	33	46.8	290	-93.0	0	38.6	200	26.1	0	70.1	50	94.8	0	92.3	0	121.5	380	-37.9	0	121.4	340	120.9	390
	34	44.3	330	-71.8	0	39.7	270	73.1	0	102.7	10	100.6	0	81.7	0	119.8	480	-13.7	0	121.5	420	121.5	570
	35	35.8	510	-22.3	0	40.4	170	55.4	0	94.2	10	54.8	0	27.8	0	120.2	820	-10.4	0	120.2	730	121.0	850
	36	37.5	960	-2.0	0	41.8	60	19.2	0	81.5	200	14.3	0	12.4	0	120.6	1330	-6.9	0	120.6	1160	122.3	1260
	37	33.8	20	-70.3	0	39.0	60	51.1	0	95.9	30	187.6	0	115.7	0	120.3	120	-19.6	0	121.8	120	119.7	120
	38	37.5	120	-73.2	0	39.6	90	42.6	0	88.7	20	158.7	0	122.2	0	120.6	130	-18.3	0	121.0	130	120.1	160
	39	40.3	230	-80.4	0	40.0	180	41.4	0	83.1	50	126.6	0	117.6	0	121.5	270	-17.6	0	121.2	240	120.4	330
	40	44.1	290	-57.3	0	40.2	220	86.6	0	112.7	0	123.9	0	103.8	0	117.6	280	5.1	0	120.8	280	119.9	470
	41	42.7	480	-5.1	0	38.8	40	80.2	0	114.8	0	94.3	0	60.8	0	120.2	440	21.7	0	120.6	370	120.5	550
	42	38.8	790	8.9	0	44.3	0	35.4	0	92.1	60	33.6	0	35.4	0	120.6	850	14.7	0	119.7	770	120.2	930
	43	35.2	50	-79.0	0	40.6	90	45.7	0	88.0	40	186.0	0	108.3	0	119.3	160	-33.2	0	121.2	160	120.2	180
	44	38.7	150	-81.1	0	40.6	130	43.2	0	82.8	20	154.4	0	130.4	0	118.7	230	-32.5	0	119.7	200	118.3	240
	45	38.7	270	-88.5	0	40.4	200	36.0	0	72.7	50	115.0	0	111.2	0	117.8	360	-33.8	0	120.2	340	119.5	410
	46	41.8	370	-67.4	0	41.0	310	82.6	0	99.0	10	118.4	0	94.6	0	118.2	480	-9.7	0	120.2	480	120.4	660
	47	38.2	560	-3.2	0	38.3	60	76.3	0	101.3	10	82.0	0	40.8	0	119.3	730	3.2	0	121.0	660	120.0	800
	48	35.7	840	12.8	0	44.3	0	36.0	0	81.3	120	31.1	0	22.3	0	122.1	1120	1.9	0	121.2	1040	120.6	1100

TABLE 6-10

AVERAGE TEMPERATURE AND POWER DATA

TEST POINT		79	47	80	48	78	53	49	40	50	76	77
SUN ANGLE		0	46		63		77	103	131			140
PANEL TOP (ZONES 1-15)	AVG TEMP ~°F	119.8	-24.4	119.5	-55.3	119.9	17.9	1.0	120.8	-1.8	120.2	120.0
	TOTAL POWER ~BTU/HR	12,210	0	14,111	0	16,780	7,280	7,035	19,970	7,010	19,560	18,930
PANEL BOTTOM (ZONES 16-30)	AVG TEMP ~°F	37.6	-54.0	40.9	-2.0	112.3	27.0	50.7	121.8	23.4	122.7	120.9
	TOTAL POWER ~BTU/hr	6,020	0	4000	0	8,700	0	0	4,900	0	4,410	5,410
PAYLOAD BAY DOOR (ZONES 31-48)	AVG TEMP ~°F	39.3	-33.4	40.9	50.0	91.6	84.0	63.1	120.0	-6.8	120.7	120.6
	TOTAL POWER ~BTU/hr	6,470	0	2300	0	760	0	0	8,560	0	7,860	9,460

FIGURE 6-3
EQUILIBRIUM TEMPERATURE
FOR VARIOUS SUN ANGLES

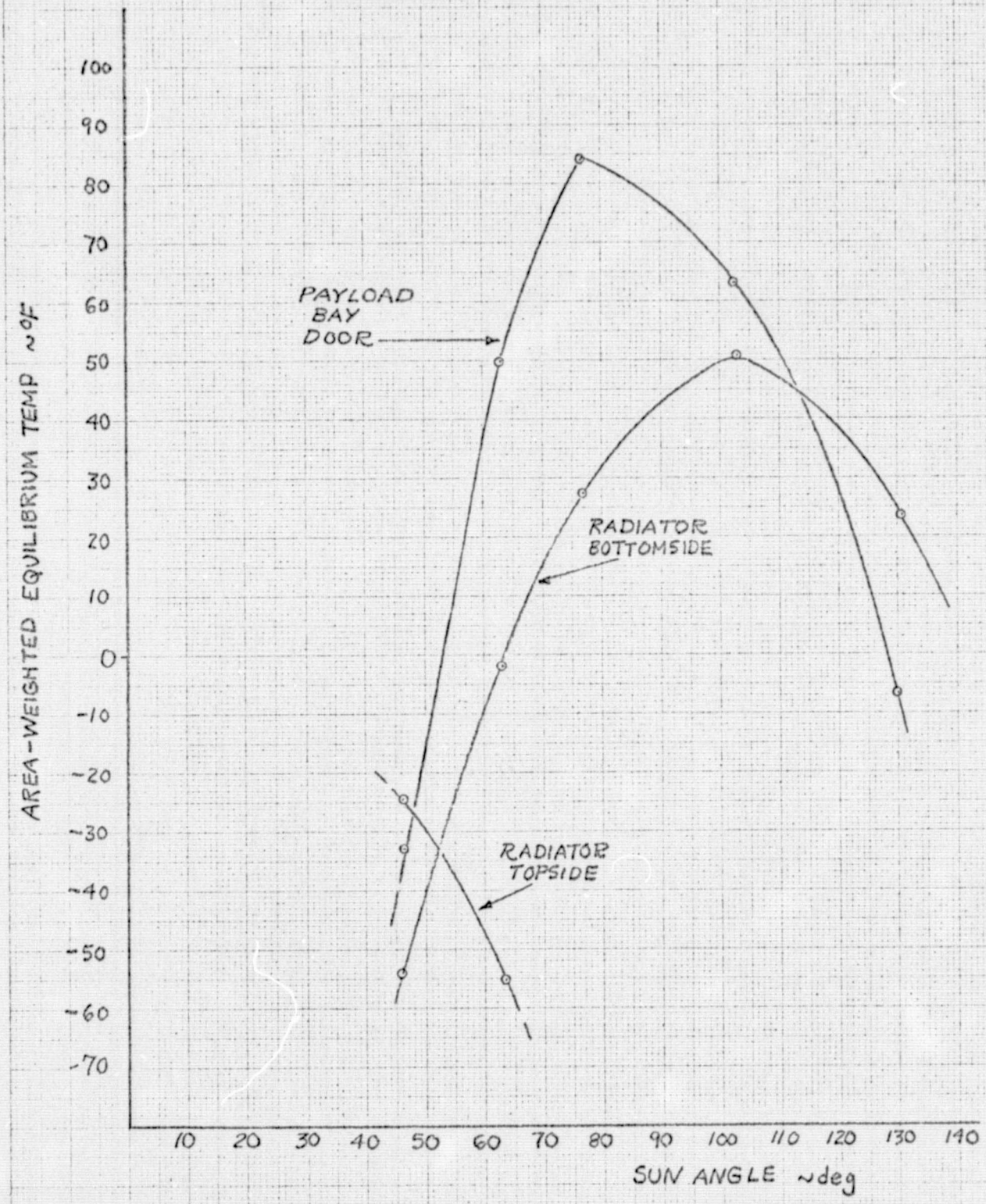

be seen that the maximum equilibrium temperature for the panel occurs at a sun angle of 103°, the position at which the cavity membrane is perpendicular to the solar beam. This distribution is indicative of minimum radiator performance in a sun-only environment.

Figure 6-4 and Table 6-11 display absorbed heat results for the panel and the payload bay door. These values are solar-only absorbed heats, with all other effects (such as door-to-panel flux) eliminated via mathematical techniques. They represent values of external environment suitable for use in a computer simulator which has the capability of calculating radiant interchange between panel and door. In prinicple, all effects of specularity are accounted for in this experimental data.

A TRASYS model was constructed to compare total absorbed heat as measured in the test with that predicted in a fully-diffuse model. Figure 6-5 presents these results. The absorptivity of the silver-Teflon was increased in the diffuse model until a reasonably good match between predicted and measured data was obtained. The value of α=.15 gave the best fit of experimental data, and is thus the effective absorptivity required to match test data.

The TRASYS model, with α=.15, however, does not provide good distributional flux information. Table 6-12 compares the measured flux on each of the five panel strips with the TRASYS prediction. Whereas the total absorbed heat is closely matched, the test data demonstrates the postulated "focusing" of energy deep into the cavity. The diffuse model is unable to adequately represent this purely specular phenomenon.

6.5 DOOR COATING COMPARISON

The purpose of the door coating test was to determine if a diffuse covering on the payload bay door would result in a net performance advantage for the

FIGURE 6-4

ABSORBED SOLAR ENERGY AS FUNCTION OF SUN ANGLE

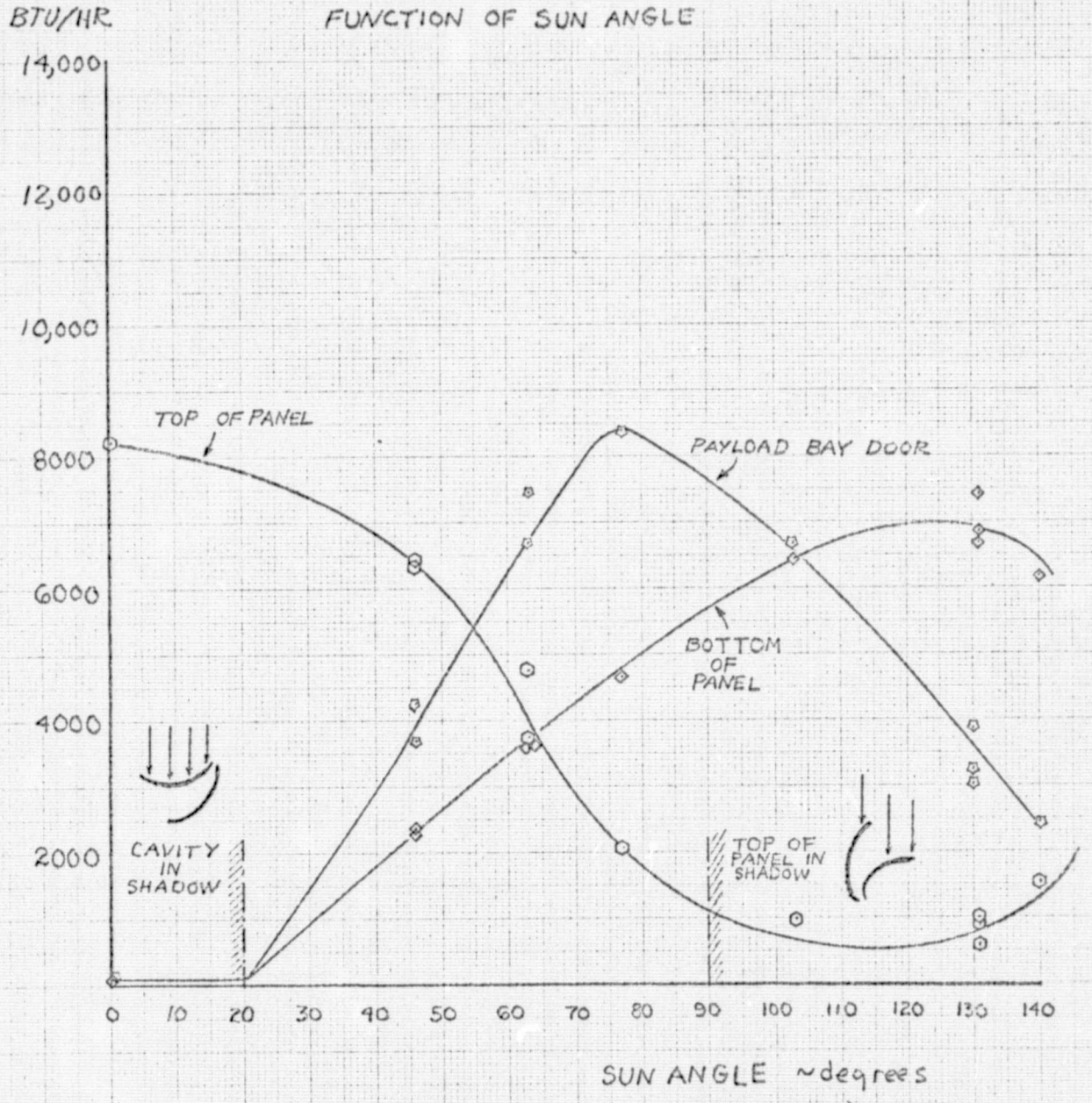

TABLE 6-11

TEST RESULTS--ABSORBED HEAT ON TEST ARTICLE

(BTU/hr)

TEST POINT	79	47	80	48	78	53	49	40	50	76	77
SUN ANGLE	0	46		63		77	103	131			140
PANEL TOPSIDE	8211	6422	6386	4756	3774	2081	984	593	882	917	1519
PANEL BOTTOMSIDE	68	2363	2341	3572	3645	4685	6458	6696	6819	7419	6114
PAYLOAD BAY DOOR	88	3657	4257	6693	7423	8390	6693	3282	3018	3880	2432
TOTAL HEAT ON PANEL BOTTOMSIDE	—	4171	4444	6878	7312	8830	9764	8317	8310	9336	7315
HEAT INCIDENT ON CAVITY +	—	25,293	25,293	35,550	35,550	41,723	46,410	40,980	40,980	40,980	37,082
EFFECTIVE ++ ABSORPTIVITY	—	.165	.176	.193	.206	.217	.210	.203	.203	.228	.200

+ HEAT INCIDENT ON CAVITY = $442\ ^{BTU}/_{HR \cdot FT^2} \times 105\ FT^2 \times \cos(103^\circ - \alpha)$ WHERE α = SUN ANGLE

++ EFFECTIVE ABSORPTIVITY = $\dfrac{\text{TOTAL ABSORBED HEAT - BOTTOMSIDE} + \text{TOTAL ABSORBED HEAT DOOR} \times \text{EXCHANGE FACTOR DOOR - PANEL}}{\text{HEAT INCIDENT ON CAVITY}}$

FIGURE 6-5

TOTAL ABSORBED HEAT - PREDICTED VS MEASURED

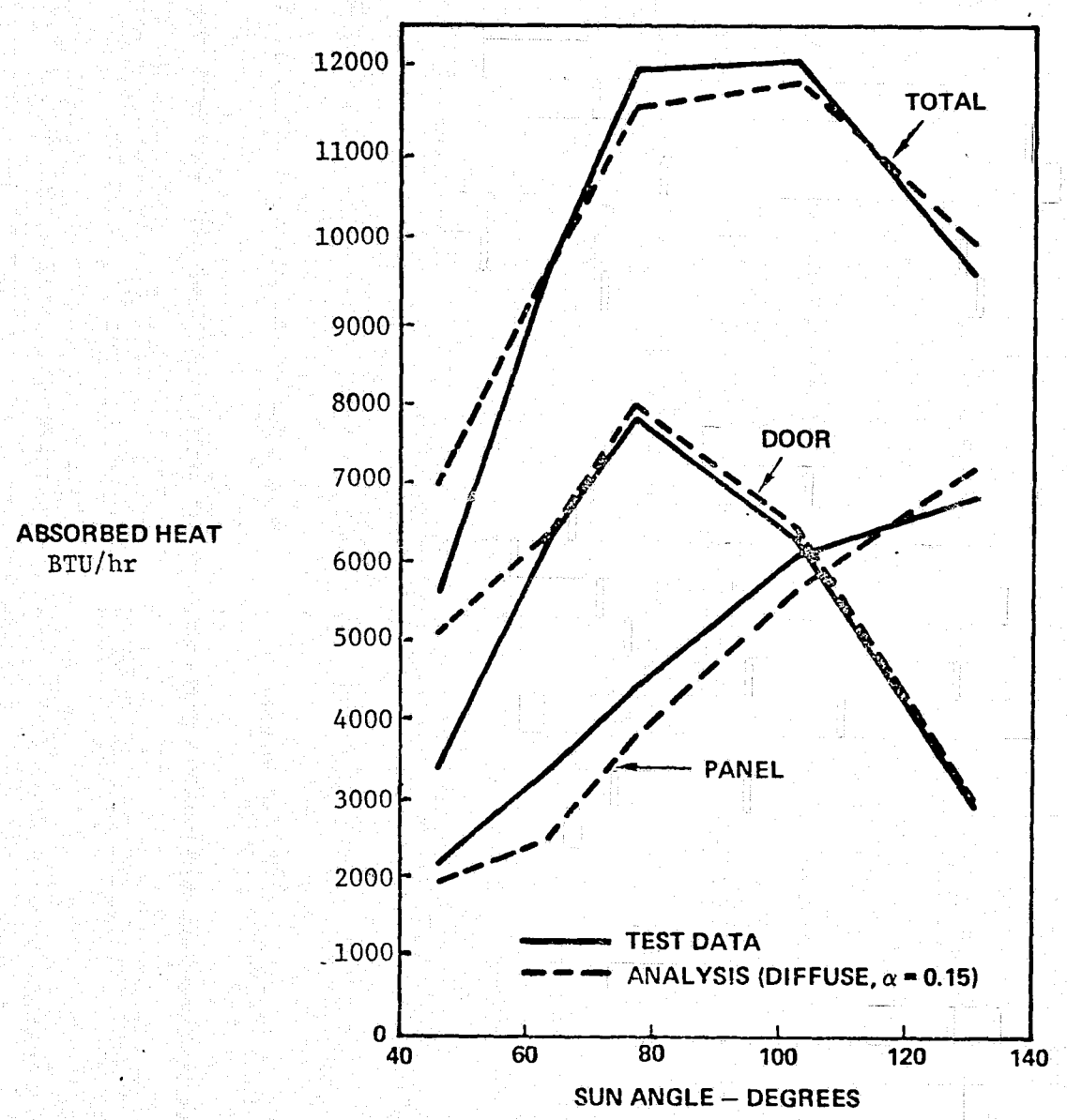

TABLE 6-12
SOLAR FLUX DISTRIBUTION ON RADIATOR PANEL
(BTU/HR/FT^2)

SUN ANGLE	FLUX	STRIP				
		6	7	8	9	10
46°	MEASURED	2.2	9.1	24.6	25.4	8.2
	PREDICTED	12.7	13.6	14.4	17.2	8.7
63°	MEASURED	12.5	53.2	68.3	7.0	5.7
	PREDICTED	6.4	17.6	28.4	23.7	8.9
77°	MEASURED	122.9	38.7	11.7	8.3	18.3
	PREDICTED	16.9	39.3	37.2	27.2	20.9
103°	MEASURED	45.9	41.1	24.3	43.9	44.1
	PREDICTED	22.2	42.9	34.5	38.3	44.6
131°	MEASURED	3.5	21.4	37.4	57.0	55.1
	PREDICTED	3.9	10.2	51.1	61.4	64.6

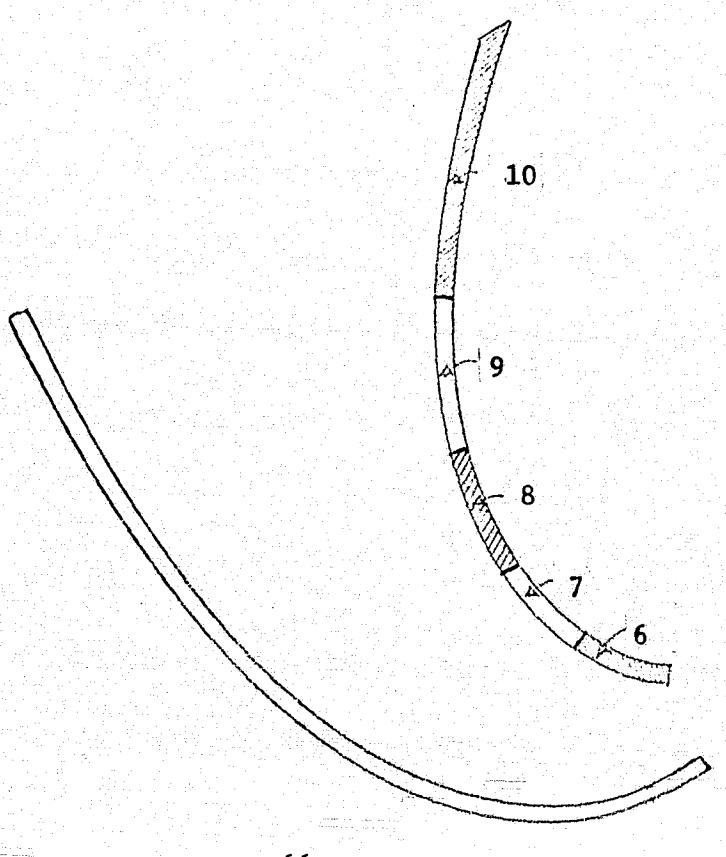

radiator panel. This advantage can be evidenced by a lower overall panel equilibrium temperature. The door was covered with a beta-cloth blanket which was more diffuse than silver-Teflon, but which was characterized by a higher ratio of solar absorptivity to IR emissivity. This higher α/ϵ causes the white door to have a higher equilibrium temperature and contribute more radiant energy to the panel at equilibrium.

Figure 6-6 and 6-7 demonstrate anticipated results. The beta-cloth door causes the maximum panel temperature to be reduced (Figure 6-6) due to the decreased focusing effect. The maximum temperature also occurs at a higher sun angle when the door is diffuse. Below a sun angle of 77°, the maximum temperature on the panel is lowered when the door is diffuse and white. However, as the sun angle increases beyond 77°, to a position in which the sun is directly incident on the underside of the panel, the diffuseness of the white door is no longer a great advantage and its higher α/ϵ causes higher equilibrium temperatures on the panel.

In Figure 6-7, the area-weighted equilibrium temperatures are compared. The beta-cloth door provides higher (and thus inferior) equilibrium temperatures than does the silver-Teflon door. The silver-Teflon advantage is the greatest when the sun is shining directly on the panel, and least when the sun is incident on the door.

Table 6-13 displays the full set of results for these door coating tests, including a set of points run with a silver-Teflon door partially covered with the beta-cloth. This "beta stripe" door was proposed as a means of achieving the best features of the silver-Teflon and beta-cloth doors. It was expected that with the beta stripe properly located, focusing could be

FIGURE 6-6

CAVITY ASSESSMENT TEST RESULTS

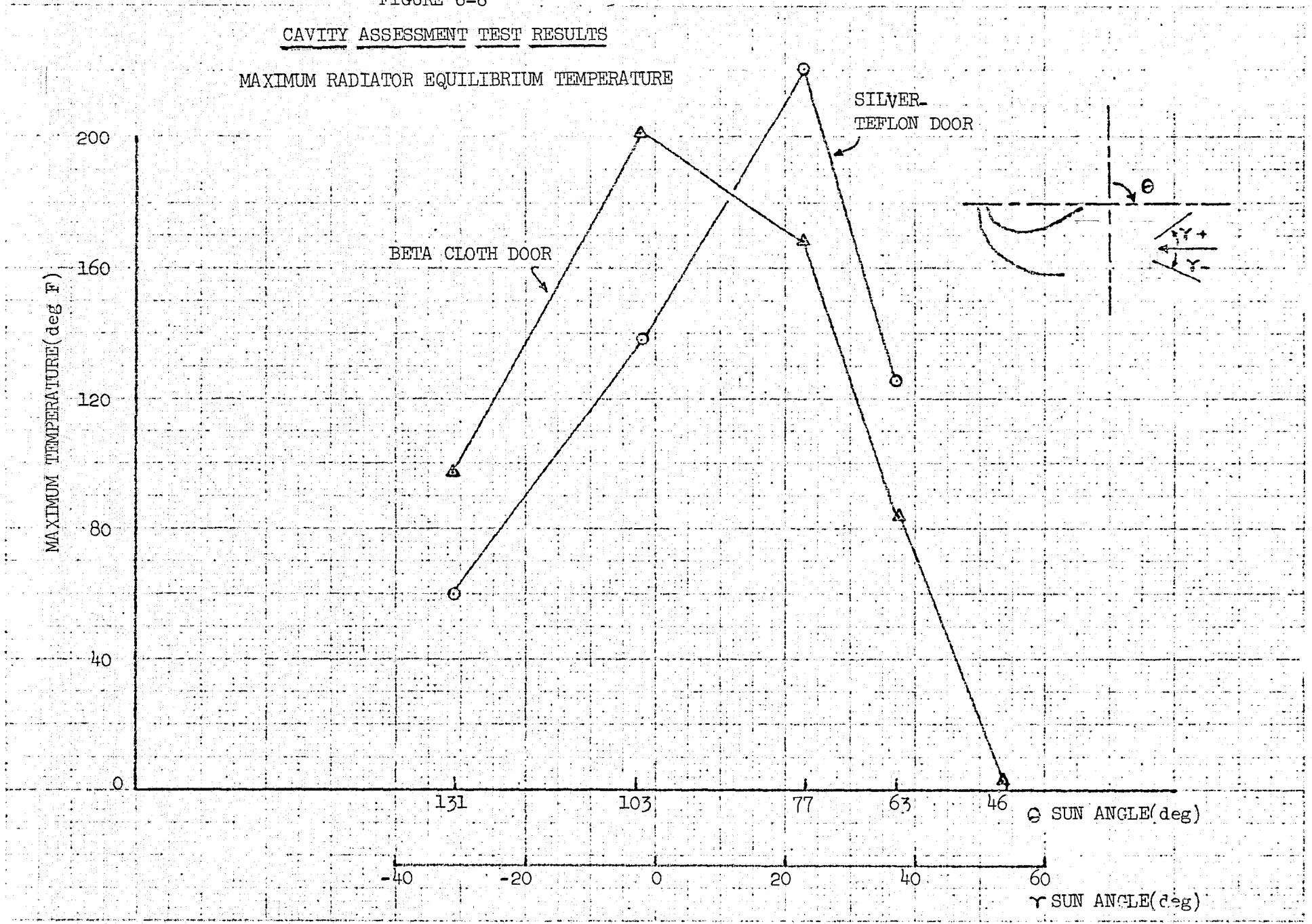

FIGURE 6-7

CAVITY ASSESSMENT TEST RESULTS

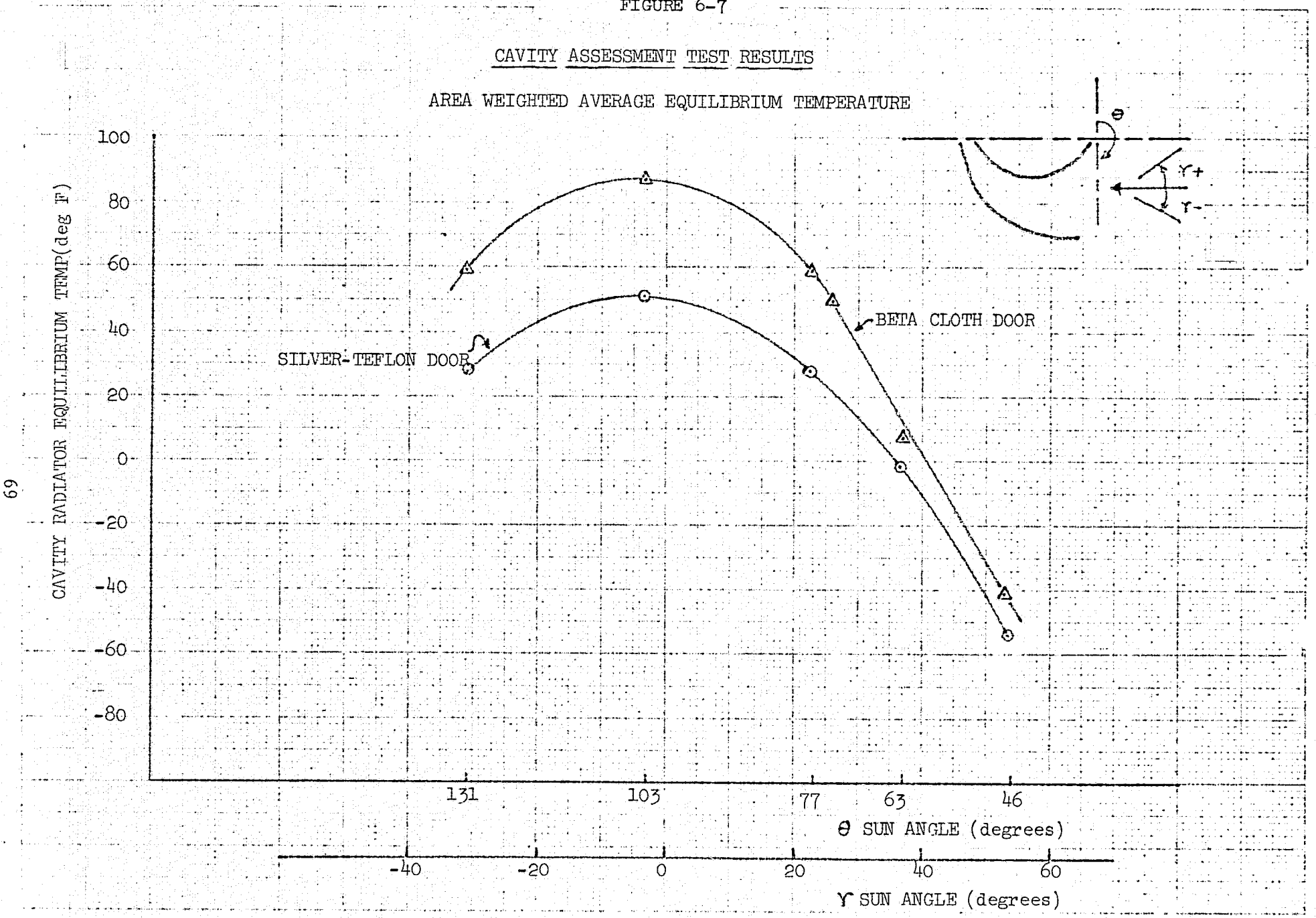

TABLE 6-13
TEST RESULTS--EQUILIBRIUM PANEL TEMPERATURES
(DEG F)

SUN ANGLE	COATING	STRIP 6	7	8	9	10	AVERAGE
46°	SILVER TEFLON	-81	-60	1.0	-4	-108	-54
	BETA CLOTH	-27	-22	-9	-13	-88	-41
63°	SILVER TEFLON	45	104	113	-11	-99	-2
	BETA CLOTH	48	63	66	28	-71	7
77°	SILVER TEFLON	206	124	56	-6	-55	27
	BETA STRIPE	126	129	96	19	-49	42
	BETA CLOTH	145	154	121	52	-24	60
103°	SILVER TEFLON	124	110	59	79	4	50
	BETA STRIPE	131	130	82	52	1	57
	BETA CLOTH	185	174	113	72	22	86
131°	SILVER TEFLON	-33	15	41	52	19	24
	BETA STRIPE	25	53	63	56	19	46
	BETA CLOTH	56	71	85	73	28	57

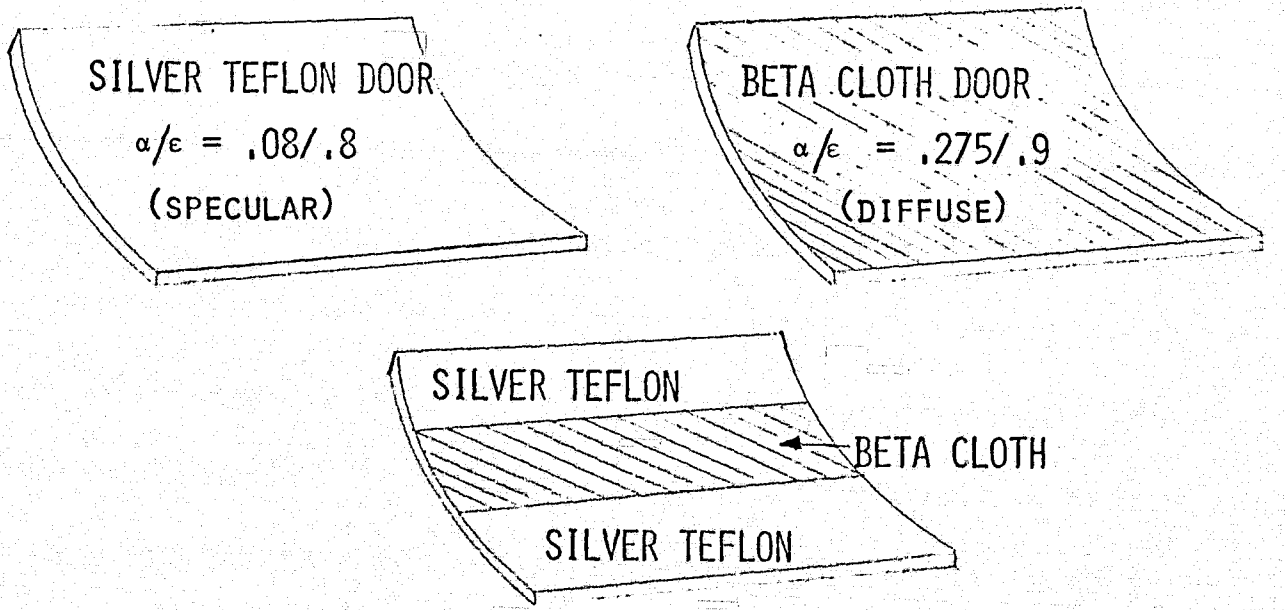

reduced without sacrificing the ability of a silver-Teflon covered door to maintain lower temperatures and consequently contribute less IR to the panel. As the results show, the beta stripe is indeed an intermediate case, significantly lowering maximum focusing effect. Nevertheless , it does produce less efficient radiator performance than the all-Teflon door.

6.6 QUARTZ LAMP CALIBRATION

The Chamber A phase of the testing was undertaken to provide data for future testing on the operation of an array of 9 quartz lamps constructed by the Space Environment Test Division personnel. Inasmuch as the array represented special test equipment, SETD personnel had the primary responsibility for data processing and analysis, however data is presented in this section to indicate the effect the QLA can be expected to have on future testing of full flowing radiator panels.

Table 6-14 presents absorbed heat data calculated for the five strips on the topside of the radiator panel simulator. The test sequence called for the SETD engineer to attempt to control the quartz lamps such that a desired average flux could be provided over the top of the test article. Due to the small thickness of the shuttle radiator panel, a simulated flux on the topside can serve as a proxy for total flux on both sides of the panel, so topside data is valuable.

As Table 6-14 shows, the higher the desired flux level, the more difficult it became to match. This phenomenon was caused by the quartz lamp emission becoming increasingly lower wavelength as the power was increased. The silver teflon coating is designed such that low wavelength radiation is reflected, and this caused it to become more difficult to increase absorbed heat by raising the temperatures of the lamps.

TABLE 6-14
HEAT ABSORBED BY TOPSIDE OF RADIATOR PANEL

TEST POINT	DESIRED FLUX BTU/HR/FT²	ABSORBED HEAT (BTU/HR) BY STRIP					TOTAL ABSORBED HEAT (BTU/HR)	AVG TOTAL FLUX BTU/HR/FT²
		1	2	3	4	5		
113	15	346	394	741	1041	1118	3640	22.5
114	30	504	395	780	1182	1581	4442	27.4
115	45	811	619	1190	1783	2417	6820	42.1
116	60	1097	815	1571	2364	3187	9034	55.8
117	75	1443	1101	2099	2730	4079	11452	70.7
118	90	1525	1117	2212	3162	4496	12512	77.2
119	105	1781	1346	2646	3760	5246	14779	91.2
120	120	2271	1766	3176	4638	6028	17879	110.4
121	135	2497	1964	3578	5183	6683	19905	122.8

Table 6-15 and Figures 6-8 and 6-9 give absorbed heat data in the cavity for constant zone temperatures(40°) and variable IR panel temperatures. The absorption from the IR panel is approximately a logarithmic function of the IR panel temperature as expressed in degrees F, which represents a testing convenience if this configuration is utilized for future testing. Analysis of this data can also be of value in the determination of environment trapping in earth oriented situations in which earth IR is the principle component of the environment.

TABLE 6-15

HEAT ABSORBED BY CAVITY

ALL ZONES 40°

TEST PT. / STRIP	ABSORBED HEAT ~ BTU/HR				
	113	114	115	116	117
IR PANEL TEMP ~ °F	20	0	-20	-40	-60
6	65	62	54	57	54
7	45	37	34	34	37
8	235	202	176	149	140
9	1043	915	794	678	599
10	2690	2322	1959	1651	1410
11	53	48	34	43	29
12	338	313	293	280	268
13	342	292	263	237	197
14	495	441	379	335	303
15	852	758	662	585	529
16	1466	1307	1161	1044	928
TOTAL	7624	6697	5809	5093	4498

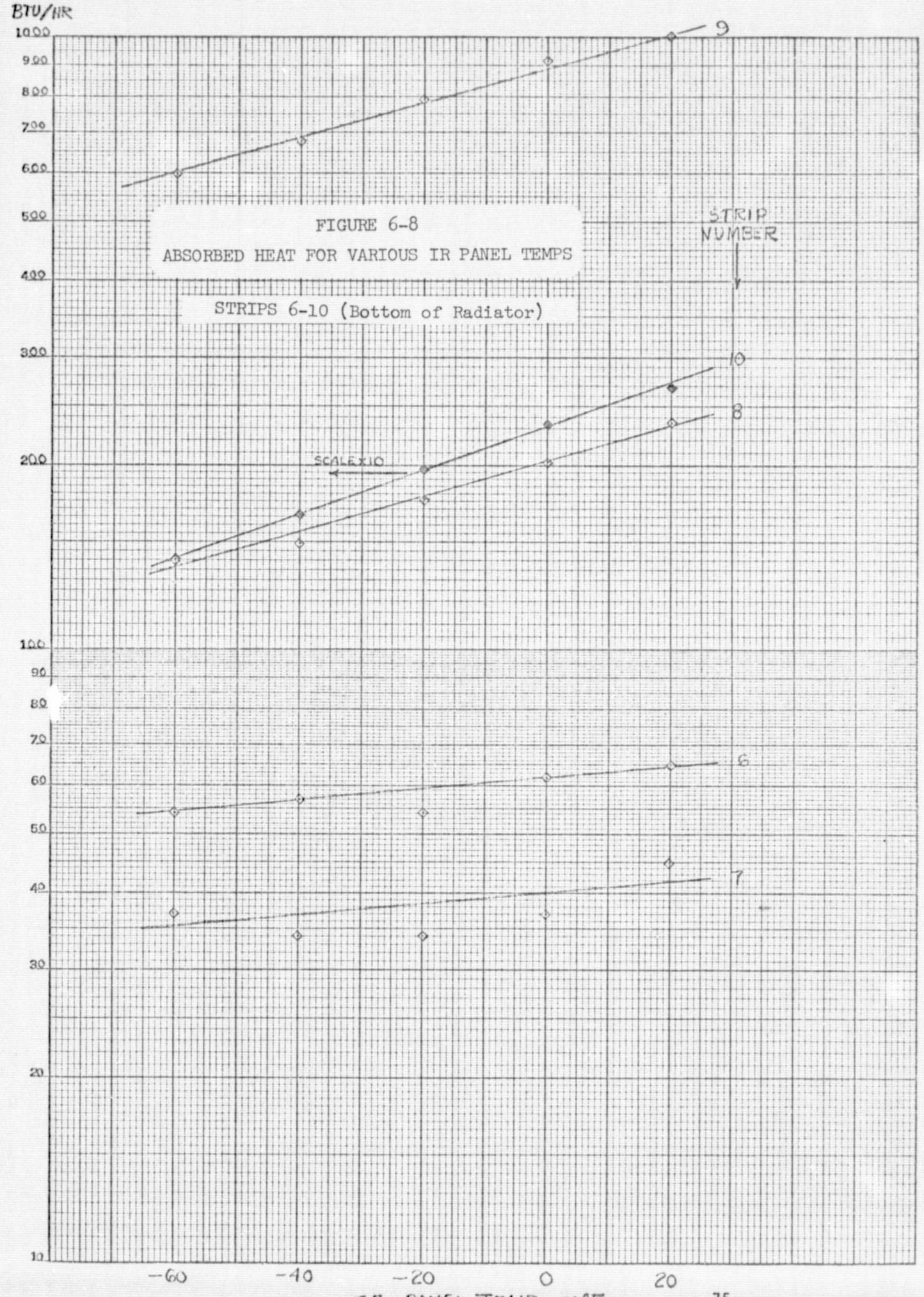

FIGURE 6-8

ABSORBED HEAT FOR VARIOUS IR PANEL TEMPS

STRIPS 6-10 (Bottom of Radiator)

KEUFFEL & ESSER CO. MADE IN U.S.A.
2 CYCLES X 140 DIVISIONS

FIGURE 6-9

ABSORBED HEAT FOR VARIOUS IR PANEL TEMPS

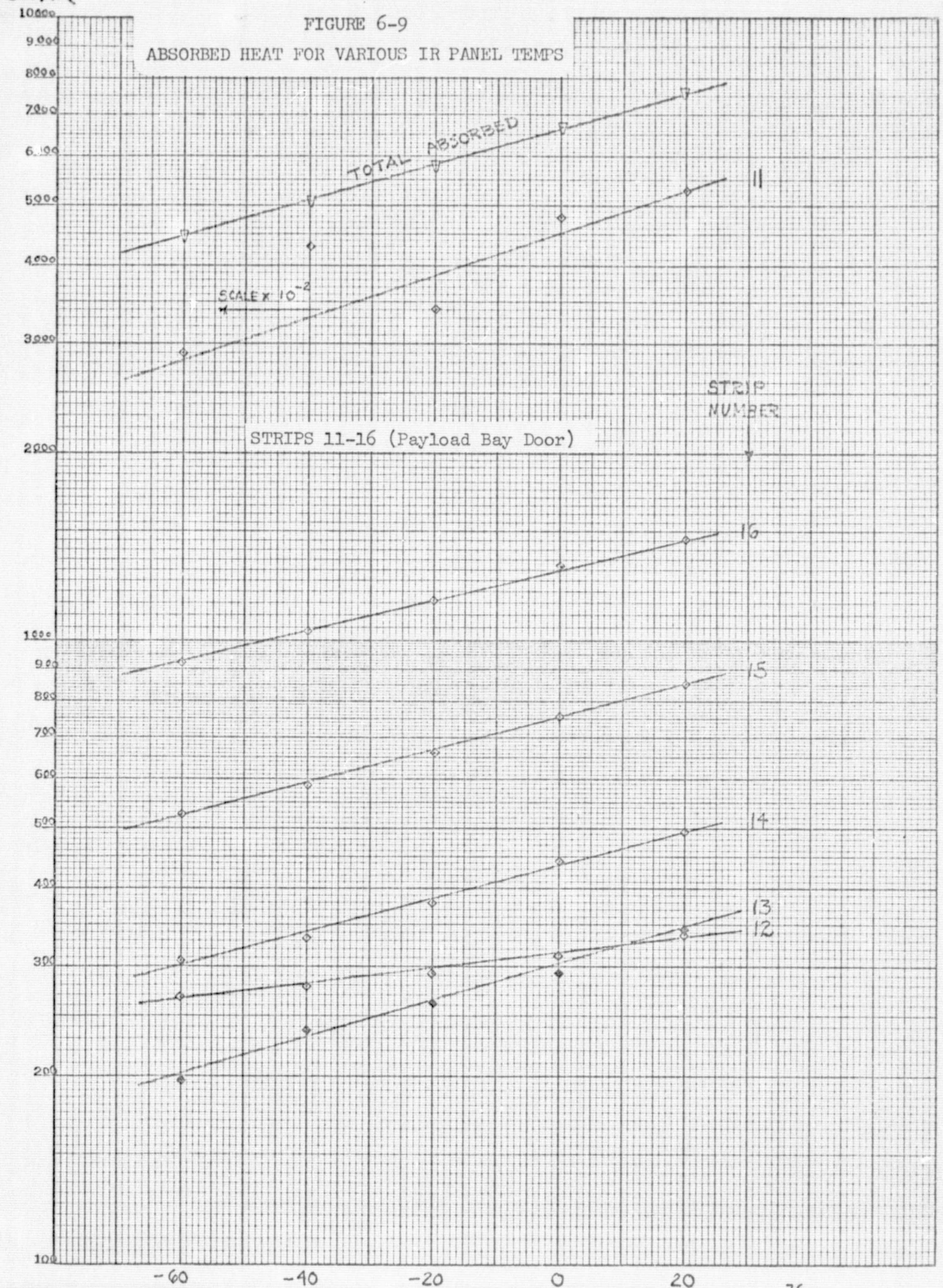

7.0 CONCLUSIONS/RECOMMENDATIONS

The specular nature of the silver/Teflon coating on the Shuttle radiator and payload bay door causes serious uncertainty in diffuse analytical prediction of radiator environments. This test program provided fundamental data on the radiation exchange factors between surfaces within the specular cavity formed by the radiator and door, which is independent of the radiator tube design. In addition, total absorbed heat on various parts of the radiator were experimentally measured in the presence of shuttle-like incident fluxes and multiple reflective surfaces.

The general confirmation that radiation trapping exists within the door/panel cavity points up the need for improved methods for calculation of environmental fluxes. Whereas diffuse analysis may be used to approximate total absorbed heat, the distributional effects of the multiple reflections cannot be duplicated in this fashion. A correlary to the need for improved specular predictive tools is a better measure of the properties of silver/Teflon including the directional aspects of its IR emissivity and solar reflectivity.

The coating applied to the payload bay door has been shown to effect the radiation absorbed by the radiator. In particular, a diffuse door coating and a part-specular, part-diffuse coating were demonstrated to be inferior to a specular coating from the standpoint of radiator performance.

APPENDIX A

RADIOMETER DATA FROM CAVITY BACKGROUND TEST

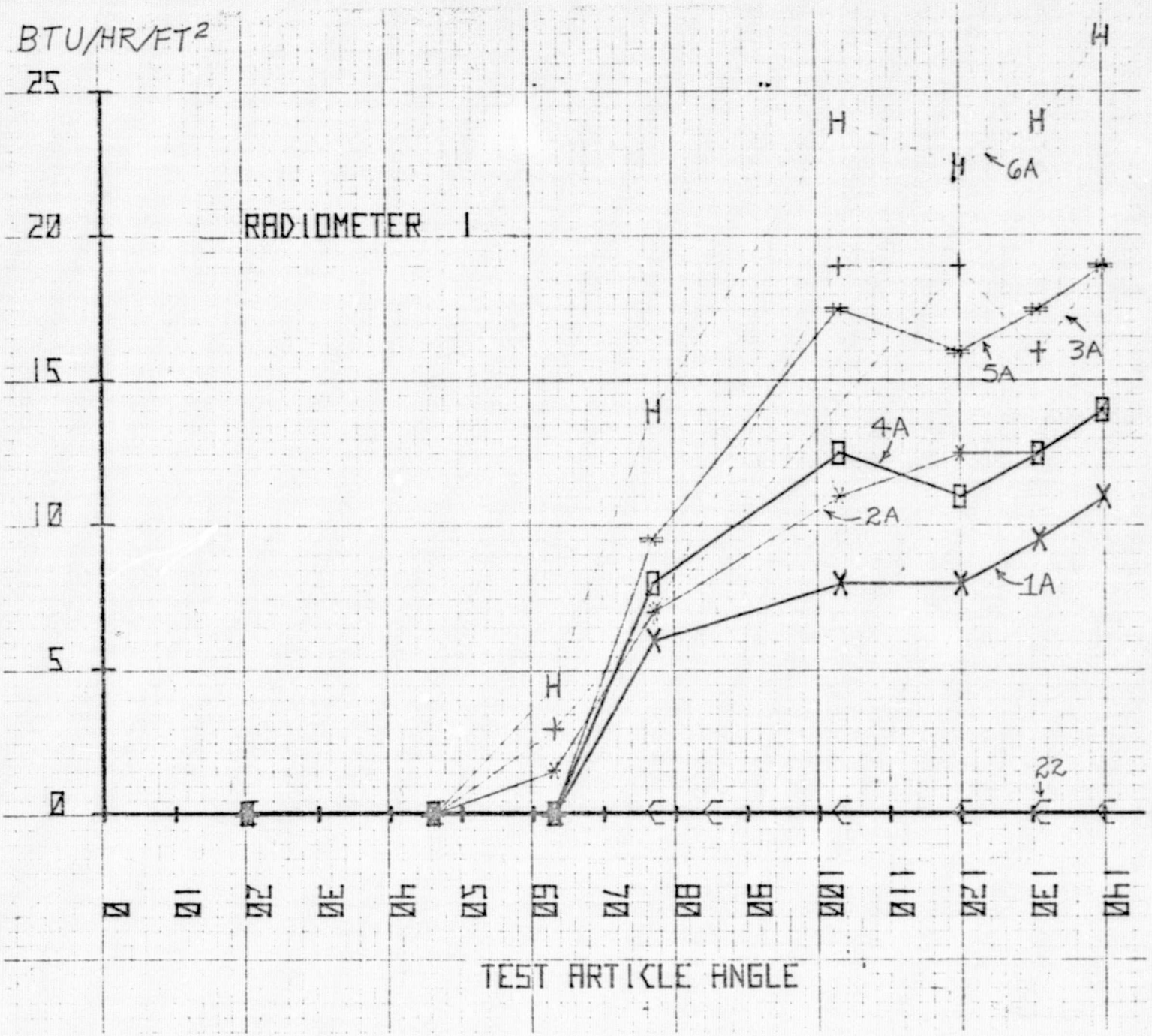
BTU/HR/FT²
25
20
15
10
5
0
RADIOMETER 1
H
6A
5A
3A
4A
2A
1A
22
0
01
02
03
04
05
06
07
08
09
10
11
12
13
14
TEST ARTICLE ANGLE

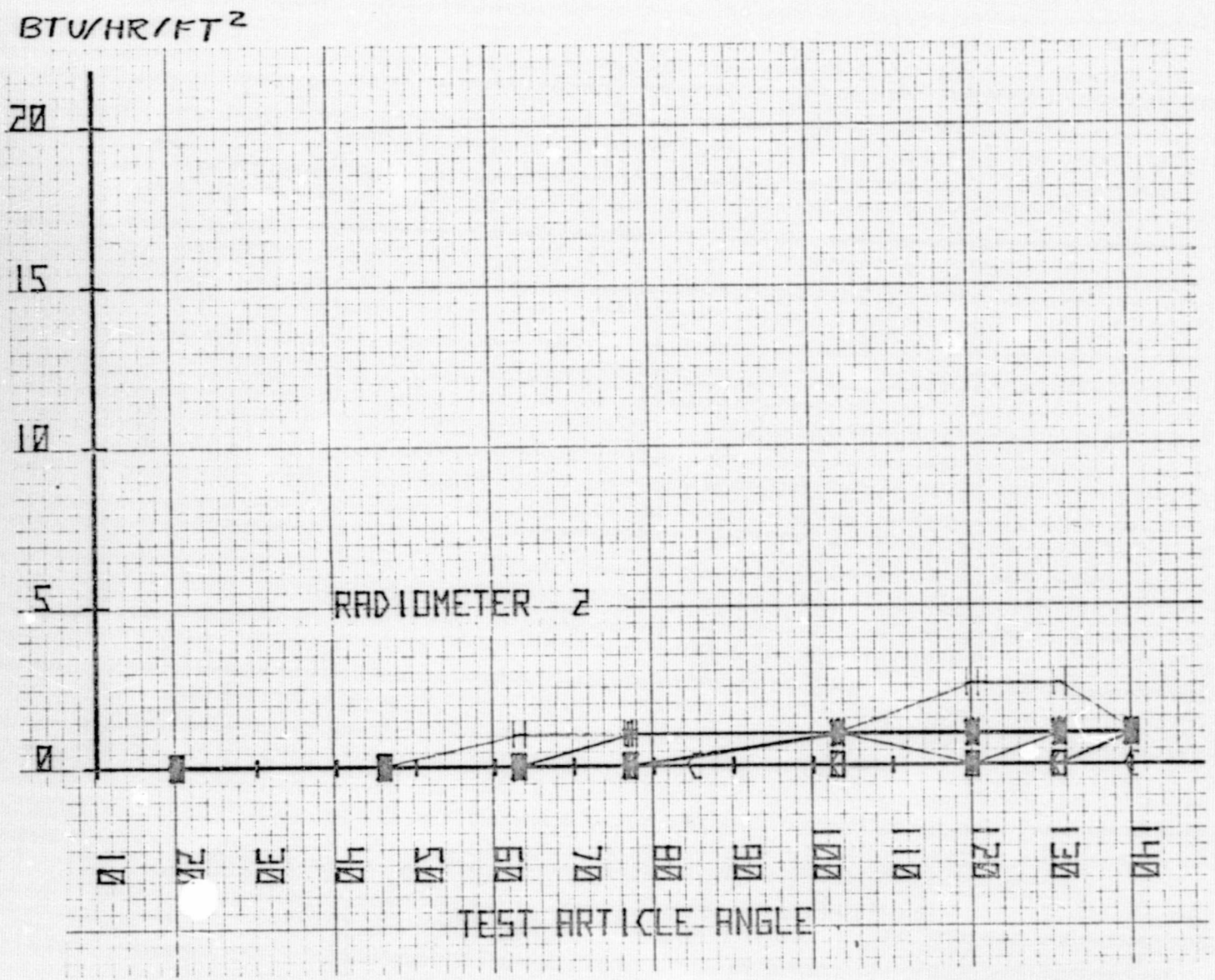
BTU/HR/FT²
20
15
10
5
0
RADIOMETER 2
01
02
03
04
05
06
07
08
09
10
11
12
13
14
TEST ARTICLE ANGLE

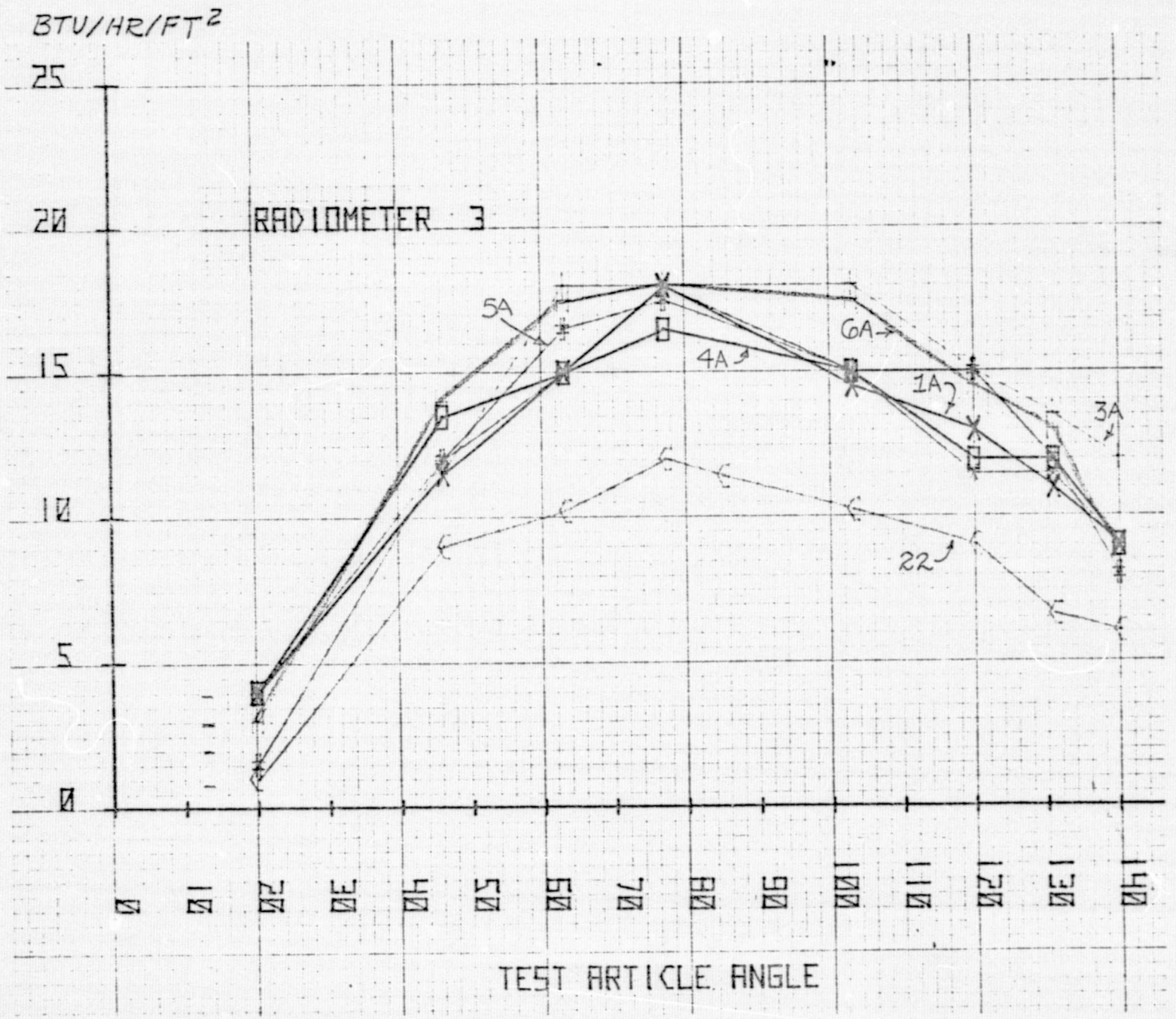
BTU/HR/FT²
25
20
15
10
5
0
RADIOMETER 3
5A
6A
4A
1A
3A
22
0
01
02
03
04
05
06
07
08
09
10
11
12
13
14
TEST ARTICLE ANGLE

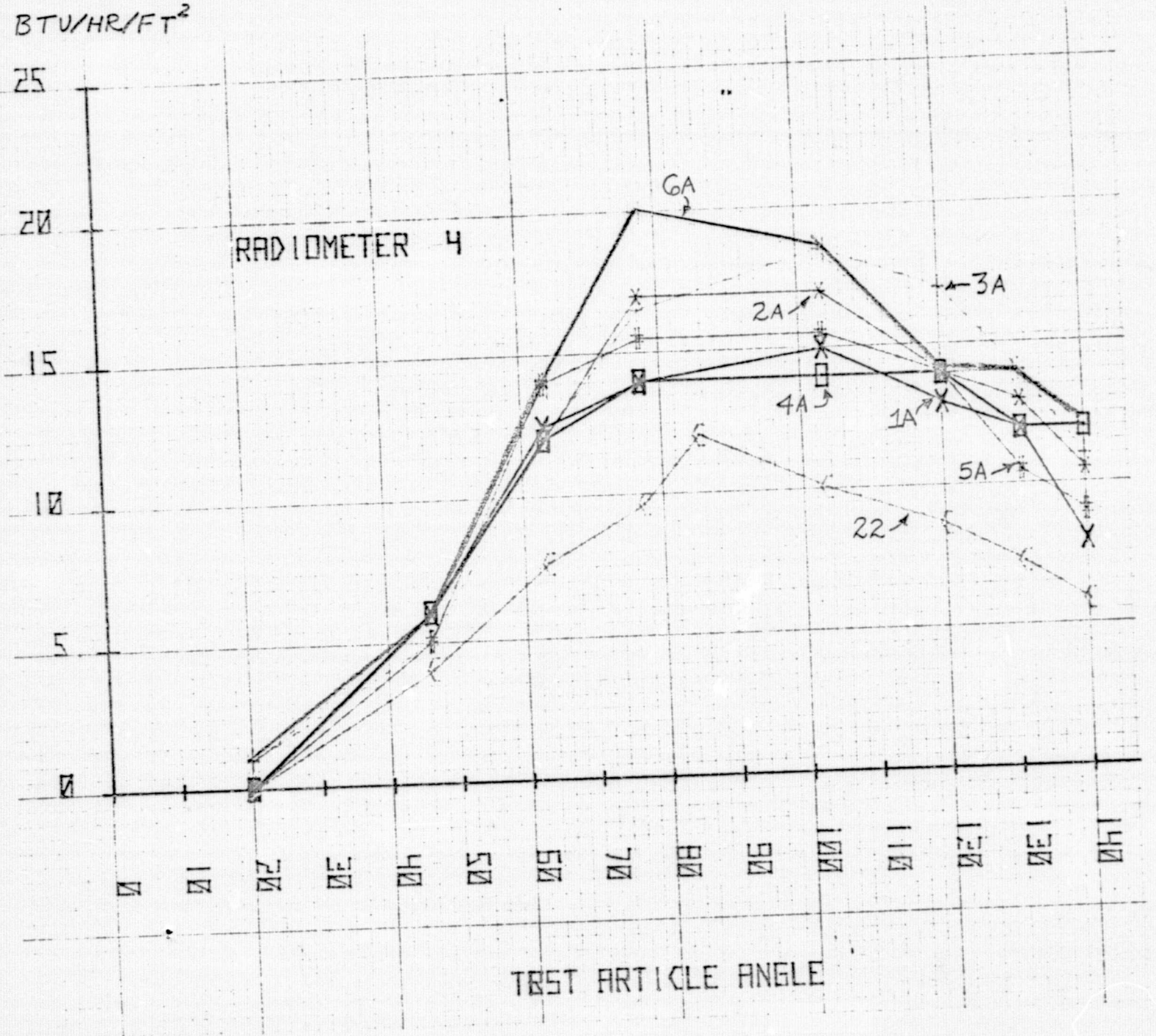
BTU/HR/FT²
25
20
15
10
5
0
RADIOMETER 4
6A
3A
2A
4A
1A
5A
22
0
01
02
03
04
05
06
07
08
09
10
11
12
13
14
TEST ARTICLE ANGLE

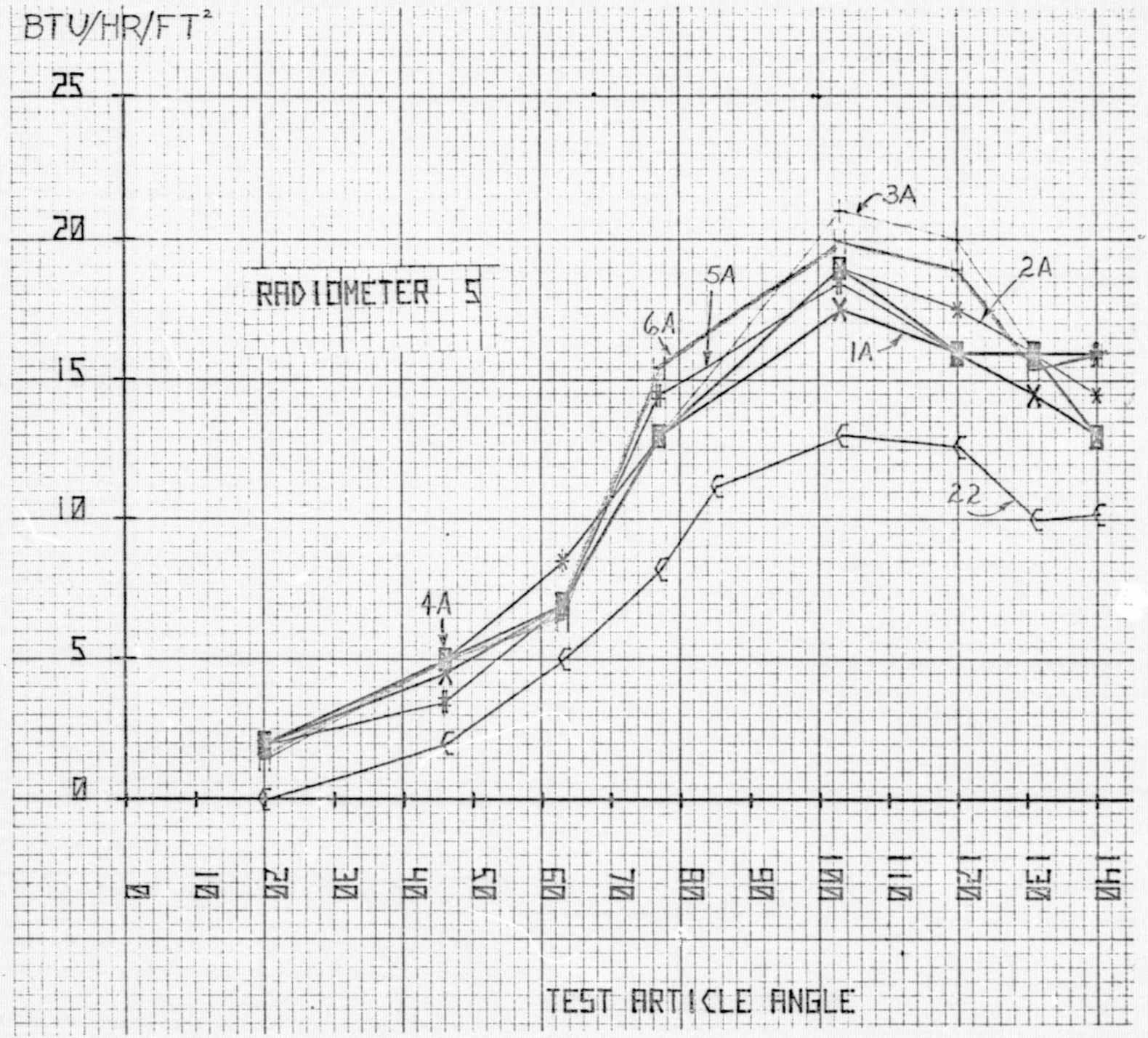
BTU/HR/FT²
25
20
15
10
5
0
RADIOMETER 5
3A
2A
5A
6A
1A
4A
22
0
10
20
30
40
50
60
70
80
90
100
110
120
130
140
TEST ARTICLE ANGLE

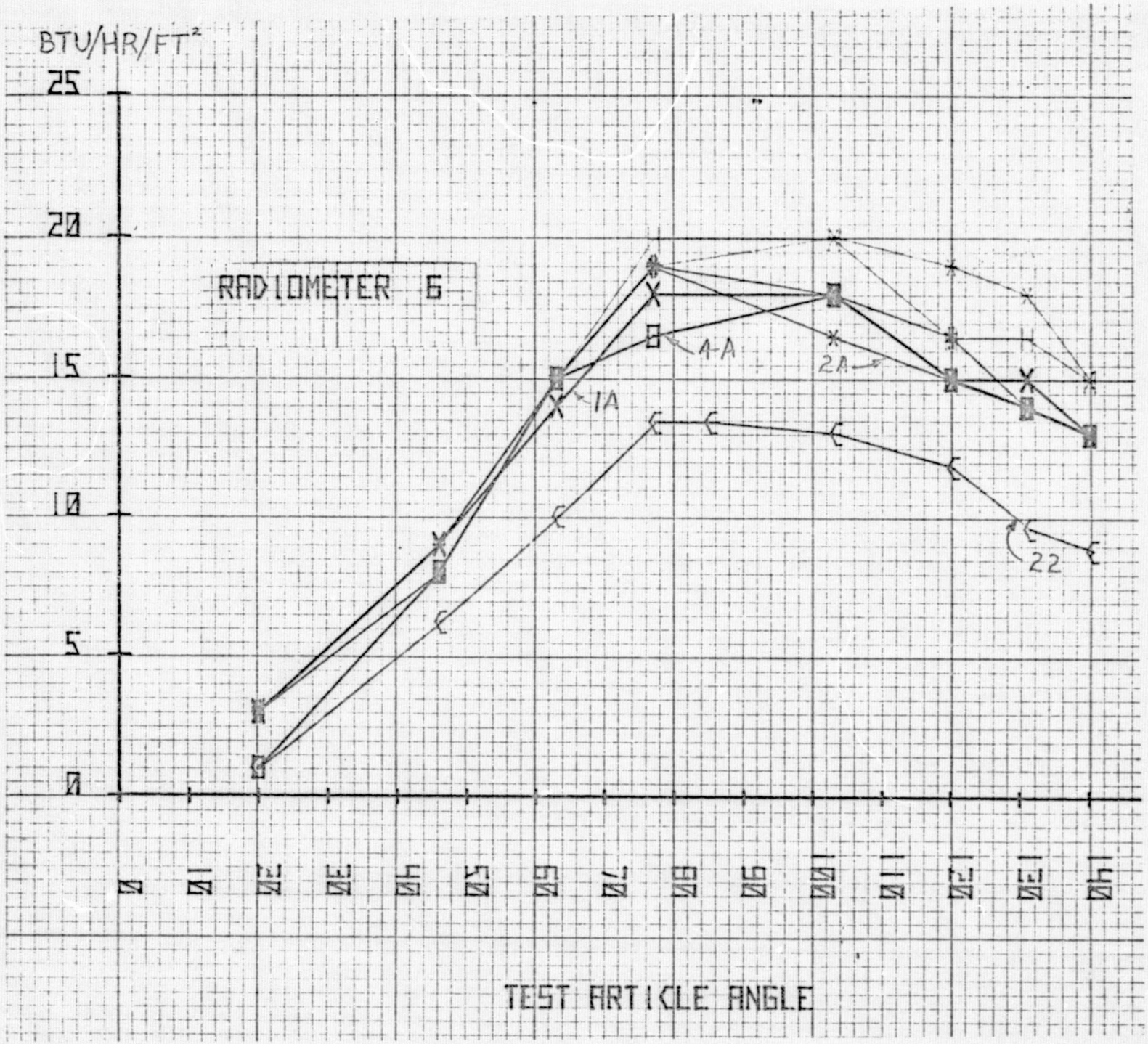
BTU/HR/FT²
25
20
15
10
5
0
RADIOMETER 6
1A
4A
2A
22
0
01
02
03
04
05
06
07
08
09
10
11
12
13
14
TEST ARTICLE ANGLE

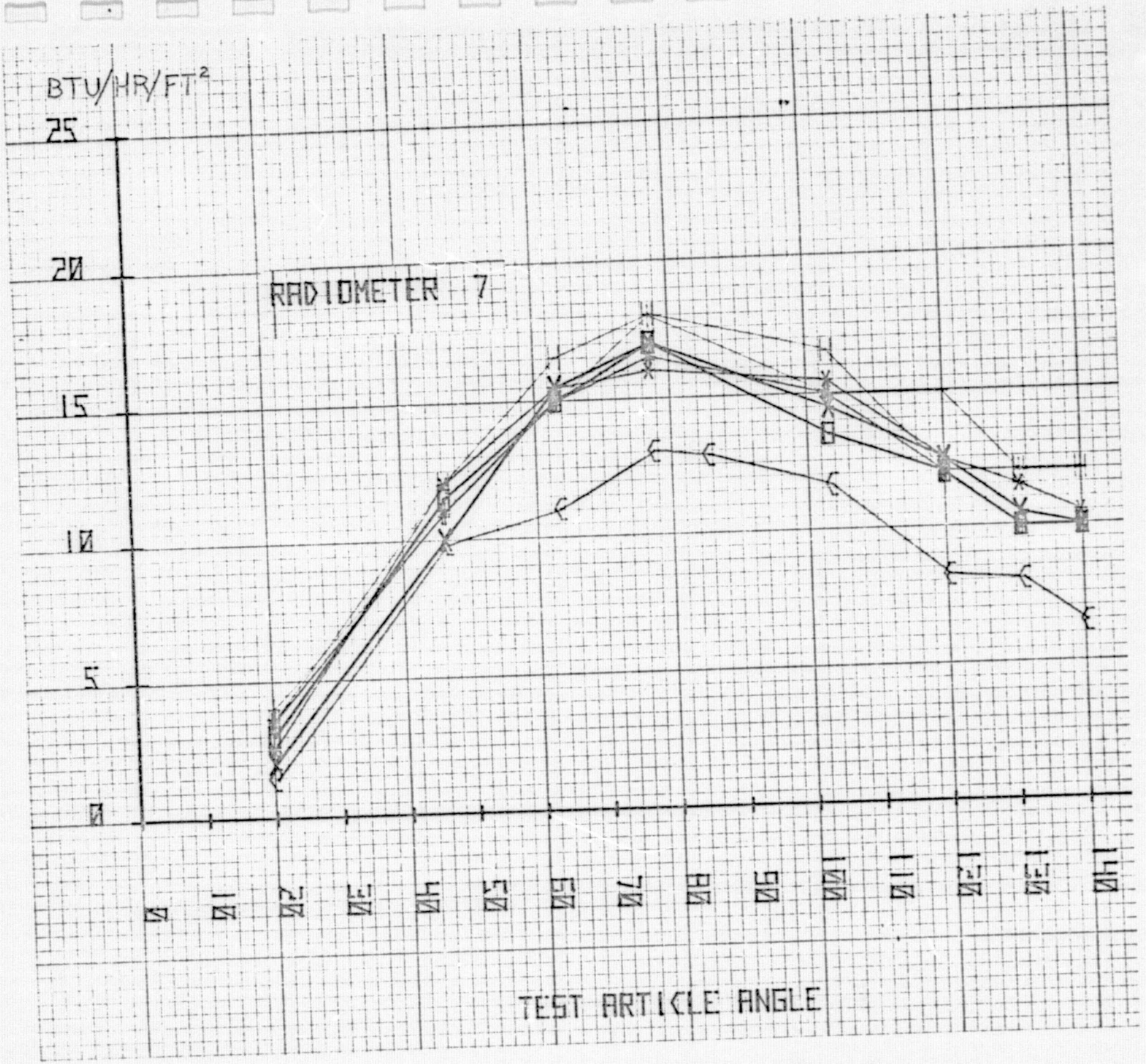
BTU/HR/FT²
25
20
15
10
5
0
RADIOMETER 7
0
10
20
30
40
50
60
70
80
90
100
110
120
130
140
TEST ARTICLE ANGLE

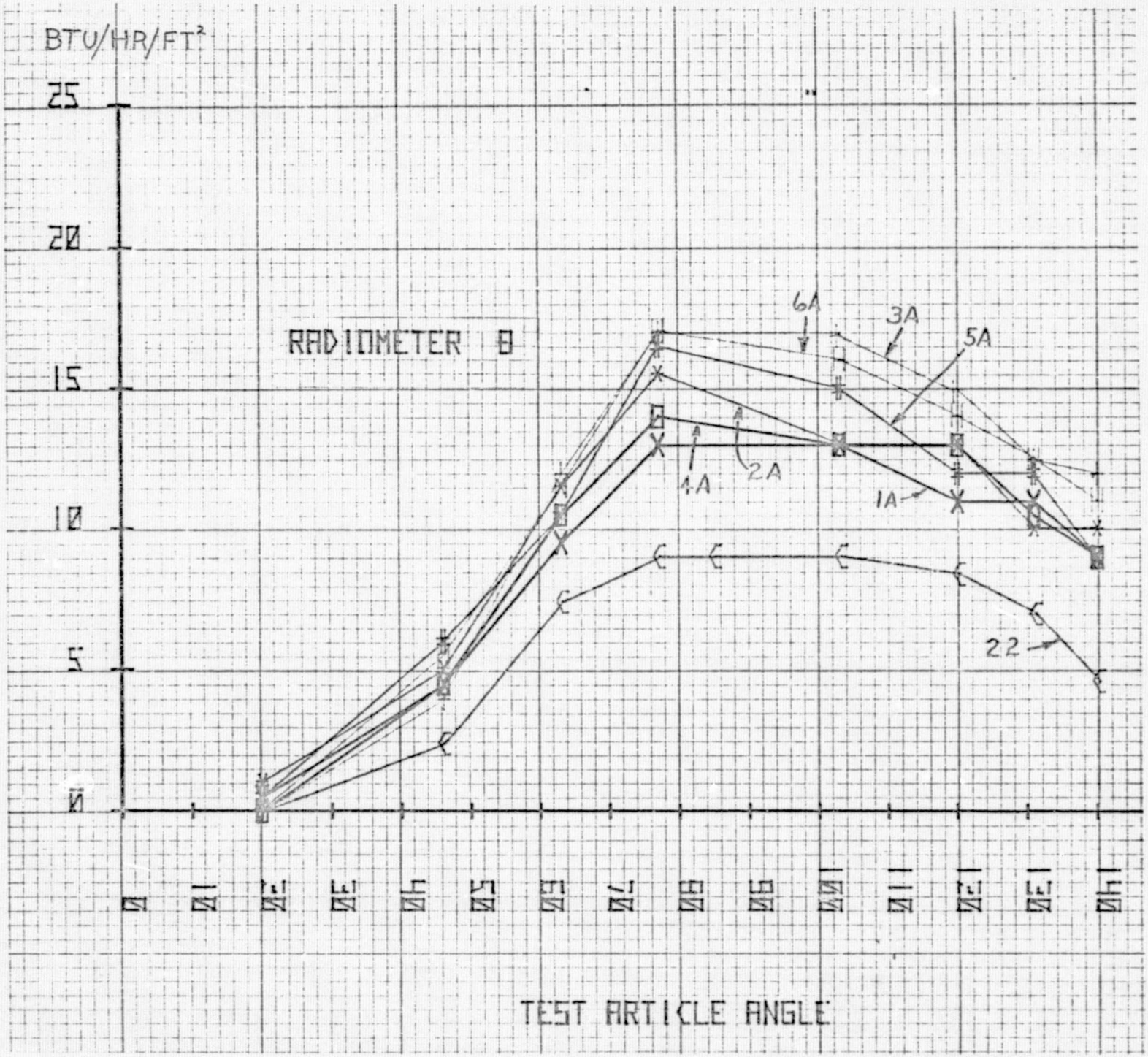
BTU/HR/FT²
25
20
15
10
5
0
RADIOMETER B
6A
3A
5A
4A
2A
1A
22
0
10
20
30
40
50
60
70
80
90
100
110
120
130
140
TEST ARTICLE ANGLE

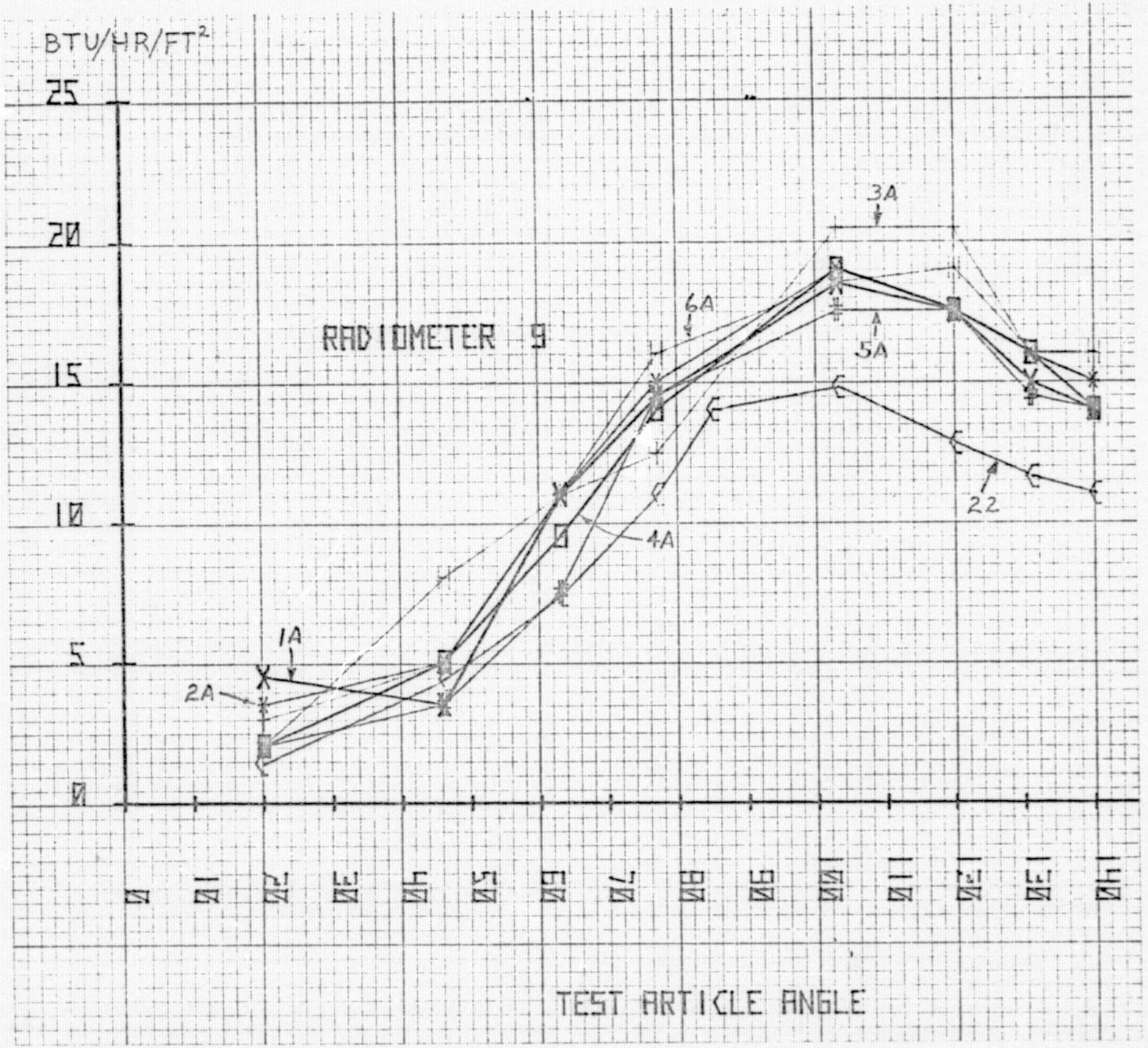
BTU/HR/FT²
25
20
15
10
5
0
RADIOMETER 9
1A
2A
3A
4A
5A
6A
22
0
10
20
30
40
50
60
70
80
90
100
110
120
130
140
TEST ARTICLE ANGLE

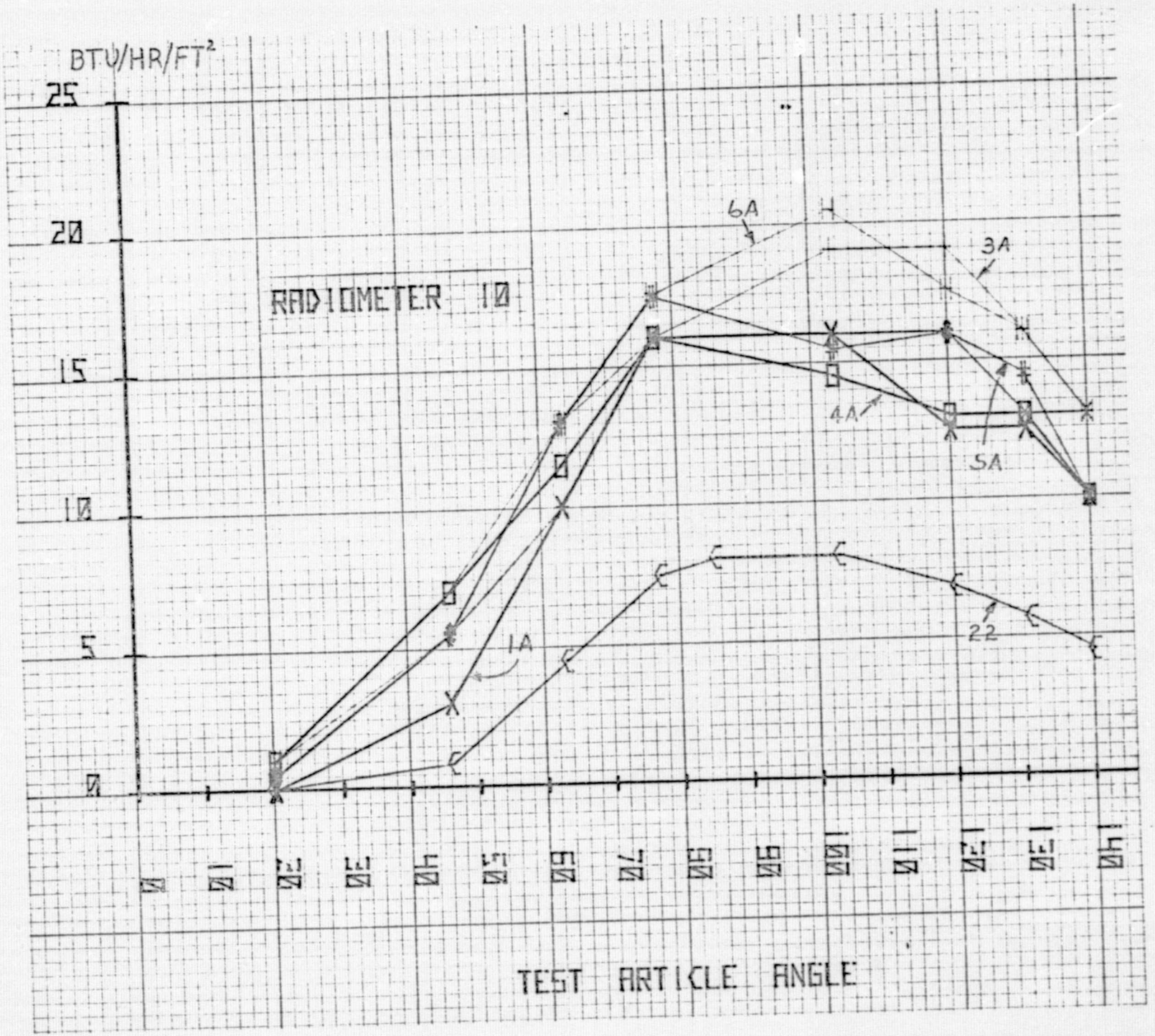
BTU/HR/FT²
25
20
15
10
5
0
RADIOMETER 10
6A
3A
4A
5A
1A
22
TEST ARTICLE ANGLE

APPENDIX B

COMPARISON OF MARCH AND JUNE TEST DATA

COMPARISON OF MARCH AND JUNE TEST RESULTS

Equilibrium panel and door temperatures recorded during the June 1975 retest differed significantly from temperatures observed in March under similar conditions. In general, the panel came to equilibrium at lower temperatures in June than had been observed in March. Table B-1 summarizes the equilibrium temperatures by strips for the two tests.

The following table demonstrates that the IR properties of the panel remained reasonably constant between March and June:

	Exchange Factor to Chamber ∿ °F		
	March (Test Point 2)	June (Test Point 4)	Change
Entire panel	58.40	55.53	-4.9%
Entire door	61.41	57.76	-5.9%
Door and panel	119.81	113.28	-5.5%
Left side zones	42.41	39.86	-6.0%
Right side zones	42.73	40.52	-5.2%
Middle zones	34.67	32.90	-5.1%

TABLE B-1

COMPARISON OF MARCH AND JUNE DATA
EQUILIBRIUM TEMPS ~ °F

STRIP	46 DEG		77 DEG		103 DEG		131 DEG	
	MARCH	JUNE	MARCH	JUNE	MARCH	JUNE	MARCH	JUNE
6	-81	-80	206	152	124	92	-33	-38
7	-60	-63	124	87	110	78	15	-7
8	1	-25	56	51	59	46	41	27
9	-4	-16	-6	-14	79	30	52	35
10	-108	-102	-55	-54	4	-6	19	7
11	-79	-75	181	149	104	82	-30	-35
12	-82	-79	147	119	119	99	-30	-35
13	-87	-85	114	82	107	80	-28	-36
14	-66	-72	114	89	94	72	-5	-17
15	-10	-30	74	54	42	26	7	-4
16	1	-12	26	15	23	12	6	-6

Various explanations for the anamoly were advanced and investigated. Among these were the following:

1. Solar lamps at higher intensity in March than June
2. Test article angle slightly different
3. Delamination of silver teflon
4. TV camera (removed in June) provided source of additional heat in March
5. Radimeters (added in June) caused solar blockage
6. Modified insulation caused less reflection
7. Computer calibration change
8. Portion of coldwall not operable in March
9. Position of test article modified between tests
10. Cleaning of columnators between tests lowered IR emissivity of solar lamps.

Each of these arguments for lower June temperatures was dismissed after investigation. The only explanation that seemed capable of explaining the observed data was a change in either solar absorptance or specularity of the silver teflon. No satisfactory explanation for this property change was discovered although the test article was moved several times and inadvertently sprinkled with water between the tests. The more conservative March data was used for absorbed heat calculations.